NEA/NSC/DOC(96)24
INDC(Ger)-042
Jül-3246

PROGRESS REPORT ON NUCLEAR DATA RESEARCH IN THE FEDERAL REPUBLIC OF GERMANY

for the Period April 1, 1995 to March 31, 1996

July 1996

Edited by
S. M. Qaim
Forschungszentrum Jülich GmbH
Institut für Nuklearchemie
Jülich, Federal Republic of Germany

CONTENTS

FORSCHUNGSZENTRUM KARLSRUHE
INSTITUT FÜR KERNPHYSIK

INSTITUT FÜR NUKLEARCHEMIE
FORSCHUNGSZENTRUM JÜLICH

INSTITUT FÜR KERN- UND TEILCHENPHYSIK
TECHNISCHE UNIVERSITÄT DRESDEN

ABTEILUNG NUKLEARCHEMIE
UNIVERSITÄT ZU KÖLN
AND
ZENTRUM FÜR STRAHLENSCHUTZ UND RADIOÖKOLOGIE
UNIVERSITÄT HANNOVER

Forschungszentrum Karlsruhe
Institut für Kernphysik

1. NEUTRON CAPTURE CROSS SECTION OF ^{15}N AT STELLAR ENERGIES*

J. Meißner[1], H. Schatz[1], H. Herndl[2], M. Wiescher[1], H. Beer and F. Käppeler

The neutron capture rate of ^{15}N may be of considerable importance for s–process nucleosynthesis in red giants as well as for the nucleosynthesis in inhomogeneous big bang scenarios. We measured the reaction cross section of ^{15}N(n,γ)^{16}N with a fast cyclic activation technique at laboratory energies of 25, 152, and 370 keV. Direct capture and shell model calculations were performed to interpret the results. The presented reaction rate is 30 to 50 % smaller than the previously used theoretical rates.

*Phys. Rev. C **53** (1996) 977

2. THE NEUTRON CAPTURE CROSS SECTION OF ^{18}O AND ITS ASTROPHYSICAL IMPLICATIONS*

J. Meißner[1], H. Schatz[1], J. Görres[1], H. Herndl[2], M. Wiescher[1], H. Beer and F. Käppeler

The neutron capture rate of ^{18}O is of considerable interest for the interpretation of nucleosynthesis in inhomogeneous big bang scenarios and for stellar helium burning in massive red giant stars as well as AGB stars. We measured the reaction cross section of ^{18}O(n,γ)^{19}O with a fast cyclic activation technique at laboratory energies of 25, 129, 152, 250, and 370 keV. Direct capture and shell model calculations were performed to interpret the results as well as previous unpublished data. Contributions to the reaction cross section and to the new stellar rate will be discussed.

*Phys. Rev. C **53** (1996) 459

[1]Department of Physics, University of Notre Dame, Notre Dame, IN 46556, USA
[2]Technische Universität Wien, A-1040 Wien, Austria

3. THE STELLAR CROSS SECTIONS FOR $^{33}S(n,\alpha)^{30}Si$, $^{36}Cl(n,p)^{36}S$, AND $^{36}Cl(n,\alpha)^{33}P$ AND THE ORIGIN OF ^{36}S*

H. Schatz+, S. Jaag, G. Linker, R. Steininger, F. Käppeler, P.E. Koehler++[1], S.M. Graff[1], and M. Wiescher[2]

The cross section of the $^{33}S(n,\alpha)^{30}Si$ reaction was measured in a neutron energy spectrum yielding the stellar rate for a thermal energy of kT=25 keV. For the $^{36}Cl(n,p)^{36}S$ reaction, the experiment was performed in the neutron energy range from 10 keV to 260 keV. Our new result for ^{33}S resolves the problem of a large discrepancy between two previous experiments. In case of ^{36}Cl it could be shown that the (n,α) channel is negligibly small compared to the (n,p) reaction at s–process conditions. The present results are used for a detailed discussion of a possible s–process origin of the rare neutron–rich isotope ^{36}S.

*_Phys. Rev. C_ **51** (1995) 379

+present address: University of Notre Dame, Notre Dame, IN 46556, USA
++present address: Oak Ridge National Laboratory, Oak Ridge, TN 37830, USA

4. CROSS SECTION OF $^{36}S(n,\gamma)^{37}S$*

H. Beer, P. V. Sedyshev[3], Yu. P. Popov[3], W. Balogh[4], H. Herndl[4], H. Oberhummer[4]

At the Karlsruhe pulsed 3.75 MV Van de Graaff accelerator the $^{36}S(n,\gamma)^{37}S(5.05\,min)$ cross section was measured by the fast cyclic activation technique via the 3.103 MeV γ–ray line of the ^{37}S–decay. Samples of elemental sulfur enriched in ^{36}S by 5.933 % were irradiated between two gold foils which served as capture standards. The capture cross section was measured at the neutron energies 25, 151, 176, and 218 keV, respectively. The $^{36}S(n,\gamma)^{37}S$–cross section in the thermonuclear and thermal energy range has been calculated using the direct–capture (DC) model combined with the folding procedure used for the determination of the potentials. The non–resonant experimental data for this reaction can be reproduced excellently using this method. The input parameters of the DC–calculation (masses, Q–values, nuclear density distributions, spectroscopic factors, spin–parity assignments and excitation energies of the low–lying states of the residual nucleus) have been taken from the available experimental data.

*_Phys. Rev. C_ **52** (1995) 3442

[1]Los Alamos National Laboratory, Los Alamos, NM 87545, USA
[2]University of Notre Dame, Notre Dame, IN 46556, USA
[3]Frank Laboratory of Neutron Physics, JINR, 141980 Dubna, Moscow Region, Russia
[4]Institut für Kernphysik, Wiedner Hauptstr. 8–10, TU Wien, A–1040 Vienna, Austria

5. NEUTRON CAPTURE CROSS SECTIONS OF THE TIN ISOTOPES

K. Wisshak, F.Voss, Ch.Theis, and F. Käppeler, K. Guber[1] L. Kazakov[2], N. Kornilov[2], G. Reffo[3]

The neutron capture cross sections of ^{114}Sn, ^{115}Sn, ^{116}Sn, ^{117}Sn, ^{118}Sn, and ^{120}Sn were measured in the energy range from 3 to 225 keV at the Karlsruhe 3.75 MV Van de Graaff accelerator. Neutrons were produced via the ^{7}Li(p,n)^{7}Be reaction using a pulsed proton beam. Capture events were registered with the Karlsruhe 4π Barium Fluoride Detector. The experiment was complicated by the small (n,γ) cross sections of the proton magic tin isotopes and by the comparably low enrichment of the rare isotopes ^{114}Sn and ^{115}Sn. Despite significant corrections for capture of scattered neutrons and for isotopic impurities, the high efficiency and the spectroscopic quality of the BaF_2 detector allowed to determine the cross section ratios with overall uncertainties of 1–2%, five times smaller compared to existing data. Based on these results, Maxwellian averaged (n,γ) cross sections were calculated for thermal energies between kT = 10 keV and 100 keV. These data are used for a discussion of the solar tin abundance and for an improved determination of the isotopic s– and r–process components.

6. THE STELLAR (n,γ) CROSS SECTIONS OF THE UNSTABLE ISOTOPE ^{135}Cs

S. Jaag, F. Käppeler, G. Reffo[3], and P. Koehler[1]

The (n,γ) cross section of the unstable isotope ^{135}Cs has been measured relative to that of gold by means of the activation method. The sample was produced by ion implantation in a high resolution mass separator and irradiated in a quasi-stellar neutron spectrum for $kT = 25\,\mathrm{keV}$ using the ^{7}Li(p,n)^{7}Be reaction near threshold. The 8 % uncertainty of the resulting stellar cross section is dominated by the thermal (n,γ) cross section used for sample definition. The experimental data are complemented by a set of calculated cross sections for the Cs isotopes. The improved cross sections are used for an s-process analysis of the ^{134}Cs-branching.

7. RESONANCE NEUTRON CAPTURE IN ^{136}Ba*

F. Voß, K. Wisshak, F. Käppeler

The neutron capture cross section of ^{136}Ba, which was determined recently with the Karlsruhe 4π BaF_2 detector, has been reanalyzed in the low energy region using a shape analysis program. Parameters of 45 resonances were extracted which allow a more reliable determination of the averaged cross section below 20 keV. The results confirm our first analysis and the reported stellar cross sections. Accordingly, the results of the s–process studies based on these data remain unchanged.

---

[1]Oak Ridge National Laboratory, Oak Ridge, Tennessee 37831 , USA
[2]Institute for Physics and Power Engineering, Obninsk–Kaluga Region, Russia
[3]ENEA, Centro Dati Nucleari, Via Martiri di Monte Sole 4, I–40138 Bologna, Italy

*Phys. Rev. C **52** (1995) 1102

8. NEUTRON CAPTURE CROSS SECTIONS OF THE CERIUM ISOTOPES FOR s– and p–PROCESS STUDIES*

F. Käppeler, K. A. Toukan[1], M. Schumann , A. Mengoni[2]

The neutron capture cross sections of the stable cerium isotopes 136, 138, 140, and 142 have been measured relative to that of gold by means of the activation method. The samples were irradiated in a quasi–stellar neutron spectrum for kT = 25 keV using the ^{7}Li(p,n)^{7}Be reaction near threshold. Variation of the experimental conditions in different activations and the use of different samples allowed the reliable determination of corrections and the evaluation of systematic uncertainties. The resulting stellar cross sections can be given with uncertainties between 3% and 7%. The present data for ^{136}Ce and ^{138}Ce are the first experimental information in this mass region of relevance for p–process studies to our knowledge, whereas the new ^{142}Ce cross section allowed to resolve a previous discrepancy. The experimental results are complemented by a set of calculated cross sections for the unstable isotopes from ^{132}Ce to ^{141}Ce as well as for ^{141}Pr, ^{142}Pr, and ^{143}Pr. The improved cross sections were used in an updated s–process analysis of the Ce–Pr–Nd region that included the small branchings at ^{141}Ce and ^{142}Pr. The consequences of the resulting s abundances are discussed with respect to isotopic anomalies in meteoritic neodymium as well as for the r– and p–process residuals.

Phys. Rev. C* **53 (1996) 1397

9. NEUTRON CAPTURE CROSS SECTIONS OF THE GADOLINIUM ISOTOPES*

K. Wisshak, F. Voß, F. Käppeler, K. Guber[3], L. Kazakov[4], N. Kornilov[4], M. Uhl[5], G. Reffo[6]

The neutron capture cross sections of ^{152}Gd, ^{154}Gd, ^{155}Gd, ^{156}Gd, ^{157}Gd, and ^{158}Gd were measured in the energy range from 3 to 225 keV at the Karlsruhe 3.75 MV Van de Graaff accelerator. Neutrons were produced via the ^{7}Li(p,n)^{7}Be reaction by bombarding metallic Li targets with a pulsed proton beam. Capture events were registered with the Karlsruhe 4π Barium Fluoride Detector, which was improved by replacing crystals with high α background and by introducing a pierced crystal at zero degree with respect to the beam axis. These changes resulted in a significantly increased efficiency for capture events. The main experimental problem was that the samples of the two s–isotopes ^{152}Gd

[1]College of Engineering and Technology, The University of Jordan, Amman, Jordan
[2]ENEA, Viale Ercolani 8, I–40138 Bologna, Italy
[3]Oak Ridge National Laboratory, Oak Ridge, Tennessee 37831, USA
[4]Institute for Physics and Power Engineering, Obninsk–Kaluga Region, Russia
[5]University of Vienna, Austria (deceased)
[6]ENEA, Centro Dati Nucleari, Via Martiri di Monte Sole 4, I–40138 Bologna, Italy

and ^{154}Gd showed only relatively low enrichment. Nevertheless, the spectroscopic quality of the BaF_2 detector allowed to evaluate the corresponding corrections for isotopic impurities reliably. The cross section ratios could be determined with an overall uncertainty of typically 1%, an improvement by factors of five to ten compared to existing data. Severe discrepancies were found with respect to previous results. Maxwellian averaged neutron capture cross sections were calculated for thermal energies between kT = 10 keV and 100 keV. The new stellar cross sections were used for an updated analysis of the s–process reaction flow in the mass region between samarium and gadolinium, which is characterized by branchings at ^{151}Sm, ^{154}Eu, and ^{155}Eu. With the classical approach, the s–process temperature could be constrained corresponding to a range of thermal energies between kT=28 keV and 33 keV. The ^{152}Gd production in low mass stars was found to depend strongly on the neutron freeze–out at the end of the helium shell burning episodes.

Phys. Rev. C* **52 (1995) 2762

10. THE STELLAR (n,γ) CROSS SECTION OF THE UNSTABLE ISOTOPE ^{155}Eu*

S. Jaag and F. Käppeler

The stellar (n,γ) cross section of the comparably short–lived isotope ^{155}Eu ($t_{1/2}$ = 4.96 yr) has been experimentally determined relative to that of gold by means of the activation method. A sample containing only 3.4×10^{14} ^{155}Eu atoms was irradiated for 17 days in a quasi–stellar neutron spectrum corresponding to a thermal energy of kT = 25 keV. The cross section obtained from the induced activity yields $<\sigma v>/v_T$ = 1320±84 mb at kT = 30 keV. This result is of relevance for analyzing the abundance pattern in the s–process branchings at A = 151, 152, and 154 with respect to the temperature during helium shell burning in low mass stars.

Phys. Rev. C* **51 (1995) 3465

11. THE STELLAR (n,γ) CROSS SECTION OF THE UNSTABLE ISOTOPE ^{163}Ho AND THE ORIGIN OF ^{164}Er

S. Jaag and F. Käppeler

The stellar (n,γ) cross section of the unstable isotope ^{163}Ho ($t_{1/2}$ = 4570 yr) has been experimentally determined relative to that of gold by means of the activation method. A sample containing 6.62×10^{17} ^{163}Ho atoms was irradiated in a quasi–stellar neutron spectrum corresponding to a thermal energy of kT = 25 keV. This sample has been produced from ^{162}Er, and the remaining impurity was sufficient to determine the ^{162}Er cross section simultaneously. For ^{163}Ho, a total stellar cross section of $<\sigma v>/v_T$ = 2125 ± 95 mb at kT = 30 keV was found as the sum of the respective partial cross sections feeding the ground and isomeric states in ^{164}Ho, respectively. This value is of relevance for

analyzing the abundance pattern, and especially the production of ^{164}Er, in the s–process branchings at ^{163}Dy and ^{163}Ho in terms of the electron density during helium shell burning in low mass stars. The corresponding ^{162}Er cross section of 1624 $\pm$ 124 mb allows to test statistical model calculations on the proton rich side of the stability valley, which are used in p–process studies.

12. THE STELLAR (n,γ) CROSS SECTIONS OF ^{191}Ir AND ^{193}Ir

S. Jaag

The existing data for the keV neutron capture cross sections of the stable Ir isotopes 191 and 193 exhibit large discrepancies and have never been published in a final version [1,2]. Therefore, the stellar cross sections of these isotopes have been remeasured relative to that of gold by means of the activation method. Metallic samples were irradiated in a quasi–stellar neutron spectrum for $kT = 25$ keV using the ^{7}Li(p,n)^{7}Be reaction near threshold. The resulting stellar cross sections of ^{191}Ir and ^{193}Ir show uncertainties of 4 and 7 percent, respectively, and are in excellent agreement with the results of Macklin et al. [1].

[1] R.L. Macklin, D.M. Drake, and J.J. Malanify, Report LA-7479-MS, Los Alamos Scientific Laboratory, 1978.

[2] P.E. Koehler and F. Käppeler, in *Nuclei in the Cosmos III*, AIP Conference Proceedings 327 (Academic Press, New York 1994) p.157.

INSTITUT FÜR NUKLEARCHEMIE FORSCHUNGSZENTRUM JÜLICH

1. Fundamental Studies on Complex Particle Emission Reactions and Isomeric Cross Section Ratios

C. Nesaraja, M. Faßbender, F. Cserpák*, S. Sudár*, S.M. Qaim

In continuation of our fundamental studies on complex particle emission reactions [cf. 1,2] we performed further radiochemical investigations on the (p,^{7}Be) process on Ca, Fe, Cu and Zn over the proton energy range of 80 to 300 MeV. Irradiations for this purpose were done at Uppsala and Saturne. Attempts have been made to characterize both the emitted ^{7}Be particle and the radioactive product nuclide. The results are expected to shed some light on the relative competition between ^{7}Be and (4p3n) emission at these energies.

Continuing our studies on isomeric cross section ratios [cf. 3,4] we investigated the ^{72}Ge(n,α)^{69m,g}Zn and ^{109}Ag(n,p)^{109m,g}Pd processes from threshold to 12 MeV. The formation of the isomeric pair ^{69m,g}Zn is also under investigation in the ^{69}Ga(n,p)^{69m,g}Zn and ^{70}Zn(n,2n)^{69m,g}Zn reactions.

Measurements on the ^{93}Nb(^{3}He,2n)^{94m,g}Tc, ^{94}Mo(p,n)^{94m,g}Tc and ^{92}Mo(α,pn)^{94m,g}Tc processes had been completed some time ago. Nuclear model calculations are now underway in collaboration with the IRK Vienna (B. Strohmaier) to describe the formation of the isomeric pair ^{94m,g}Tc in several reactions.

Studies on the isomeric pair ^{58m,g}Co have been in progress for several years. Experimental and theoretical work has now been completed [cf. 5]. The isomeric cross section ratio was determined in 7 reactions, namely, (n,p), (n,2n), (p,pn), (p,n), (d,n), (p,α) and (α,n). The results are shown in Fig. 1 as a function of excitation energy of the product nucleus. The values show large differences, depending on the type of the reaction involved. The spin of the target nucleus seems to play an important role. The ratio is relatively high for target nuclei with high spin values. Furthermore, the α-particle induced reaction leads to somewhat higher isomer ratio, especially with increasing excitation energy. The effect of α-particle in the exit channel, however, is not significant.

---

* Guest scientist from Institute of Experimental Physics, Kossuth University, Debrecen, Hungary

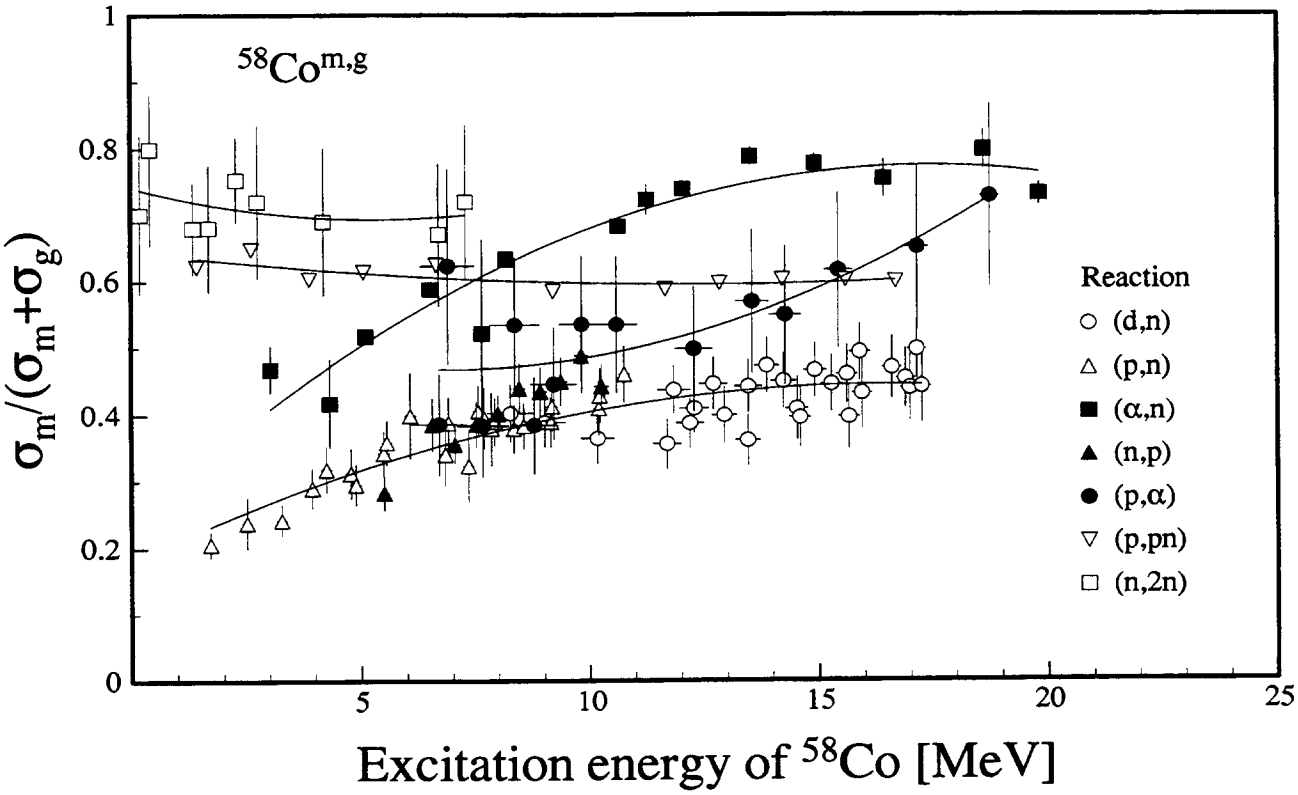

Fig. 1 Measured isomeric cross section ratios for different charged particle and neutron induced reactions plotted as a function of the maximum excitation energy of the product nucleus ^{58}Co. The curves give eye-guides to the data on each reaction (for details cf. Ref. [5]).

2. Formation of Long-Lived Activation Products in Fast Neutron Induced Reactions

S.M. Qaim, R. Klopries, St. Spellerberg, R. Dóczi*, F. Cserpák*, S. Sudar*, J. Csikai*

(Relevant to request identification numbers: 861026 R, 861027 R, 921065 R)

The continuing work on the long-lived activation products ^{108m}Ag ($T_{1/2}$ = 433 a), ^{150m}Eu ($T_{1/2}$ = 36.9 a), ^{158}Tb ($T_{1/2}$ = 180 a) and ^{63}Ni ($T_{1/2}$ = 100 a), formed via $^{109}Ag(n,2n)$, $^{151}Eu(n,2n)$, $^{159}Tb(n,2n)$ and $^{63}Cu(n,p)$ reactions, respectively, was completed [cf. 6,7]. The radioactivity of the first three products was determined non-destructively using high-resolution γ-ray spectrometry. For investigations on ^{63}Ni,

* Guest scientist from Institute of Experimental Physics, Kossuth University, Debrecen, Hungary

however, repeated anion-exchange chromatographic separation was performed and the activity determined via low-level β^- counting. The experimental data were compared with the results of statistical model calculations. The (n,2n) excitation function was described well by the model calculation. The experimental results for the $^{63}Cu(n,p)^{63}Ni$ reaction are shown in Fig. 2 together with two earlier values for 14.7 MeV neutrons. For comparison the results of four evaluations are also reproduced. All of them are based on the statistical model but the input parameters are different. Evidently, the calculational results are strongly dependent on the input parameters. Our experimental data suggest that the ADL.3 evaluation describes the excitation function of the $^{63}Cu(n,p)^{63}Ni$ reaction better than the other evaluations.

Radiochemical investigations on the $^{89}Y(n,2n)^{88}Y$ ($T_{1/2}$ = 106.6 d), $^{89}Y(n,p)^{89}Sr$ ($T_{1/2}$ = 50.6 d) and $^{89}Y(n,\alpha)^{86}Rb$ ($T_{1/2}$ = 18.7 d) reactions were also completed. Excitation functions were measured from the respective thresholds up to 14.7 MeV. Our results agree with the literature values on the (n,2n) reaction and provide the first

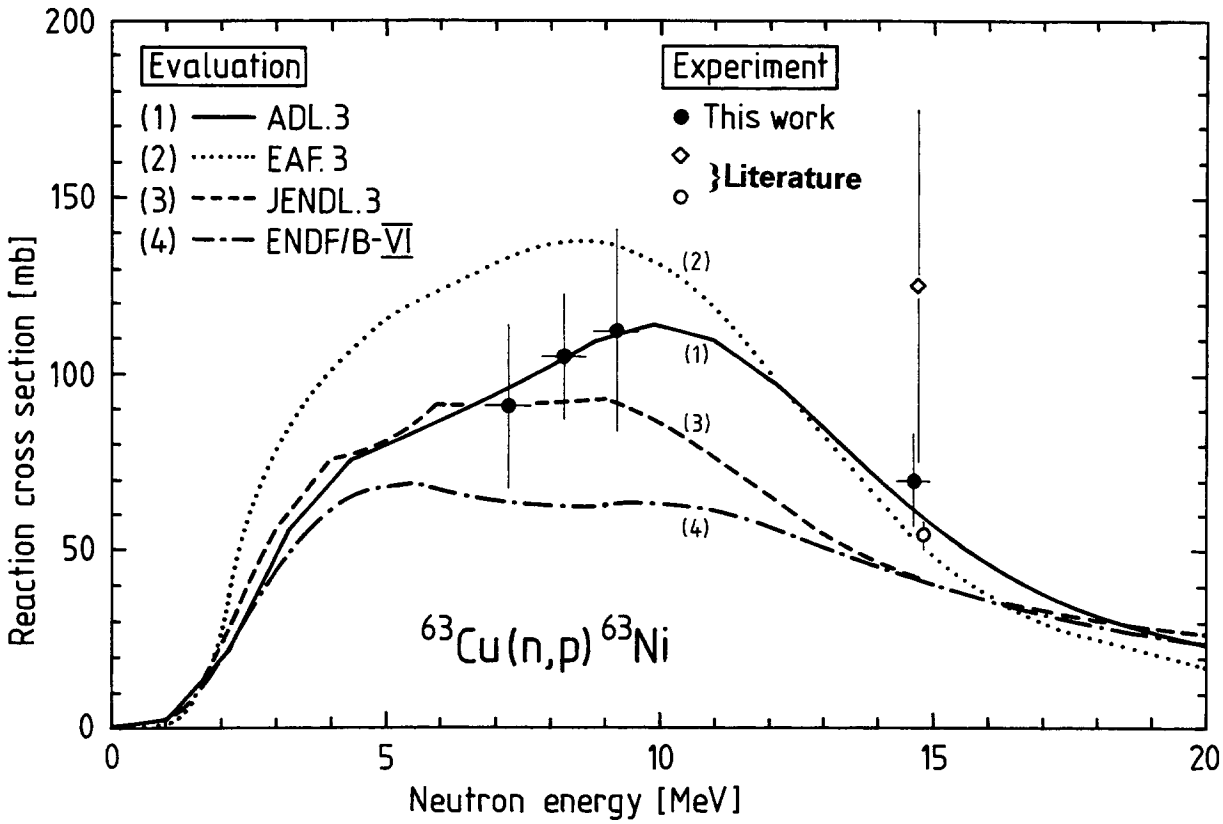

Fig. 2 Excitation function of $^{63}Cu(n,p)\ ^{63}Ni$ reaction measured radiochemically. The results of four evaluations, all based on the statistical model but with different input parameters, are also reproduced (for details cf. Ref. [7]).

consistent set of data on the (n,p) and (n,α) reactions near their thresholds. Statistical model calculations incorporating precompound effects were performed on the three excitation functions under consideration. The experimental and theoretical results were found to be in good agreement.

3. Activation Cross Section Data Relevant to Proton Therapy

M. Faßbender, B. Scholten, S.M. Qaim

Work initiated in this direction about two years ago was continued during the period of this Progress Report. Three further irradiation experiments (Uppsala and Saturne) led to more data on reactions leading to the formation of ^{7}Be, ^{22}Na, ^{24}Na and several other activation products, especially from Ca, Fe, Cu and Zn, in the proton energy range of 80 to 300 MeV. The data are being used to estimate the level of activity in the collimators after a series of therapeutic irradiations. Studies on the formation of short-lived β^+ emitters like ^{11}C ($T_{1/2}$ = 20 min), ^{15}O ($T_{1/2}$ = 2 min) and ^{18}F ($T_{1/2}$ = 110 min) in the interactions of biologically important materials with 200 MeV protons are at the planning stage.

4. Excitation Functions Relevant to Radioisotope Production

B. Scholten, F.-O. Denzler, A. Klein, A. Hohn, Z. Kovács①, Z. Szücs①, S. Takács①, F. Tárkányi①, M.R. Zaman②, R.M. Lambrecht③, F. Rösch, S.M. Qaim

In continuation of our investigations on the cyclotron production of medically interesting radioisotopes, we measured several excitation functions. The emphasis during the period of this report was on β^+ emitting radioisotopes ^{22}Na, ^{51}Mn, ^{55}Co, ^{120}I and ^{124}I, and on single photon emitters ^{99m}Tc and ^{147}Gd.

^{22}Na ($T_{1/2}$ = 2.6 a) is used for calibration of PET cameras. The most common route for its production is the $^{24}Mg(d,\alpha)^{22}Na$ process which demands a medium-sized cyclotron. We investigated the $^{22}Ne(p,n)^{22}Na$ reaction using the well-established

---

① Guest scientist from Institute of Nuclear Research of the Hungarian Academy of Sciences (ATOMKI), Debrecen, Hungary

② Guest scientist from Department of Applied Chemistry and Chemical Technology, University of Rajshahi, Rajshahi, Bangladesh

③ Scientific collaborator from PET Zentrum, Universität Tübingen, Germany

stacked-gas-cell technique. The results showed that the optimum energy range for the production of ^{22}Na is $E_p = 15 \rightarrow 6$ MeV, with the theoretical thick target yield amounting to 304 KBq (8.2 μCi)/μAh. This production method can thus be applied at a small cyclotron [cf. 8].

^{51}Mn ($T_{1/2}$ = 46 min) appears to be a suitable β^+ emitting radioisotope for in-vivo pharmakokinetic investigations via PET on the Mn-complexes used as contrast agents in Magnetic Resonance Imaging (MRI). The most promising route for its production at a compact cyclotron appears to be the $^{50}Cr(d,n)^{51}Mn$ process. However, since the radioisotope decays exclusively via β^+ emission, without any characteristic γ-ray associated with it, the measurement of excitation function presented some difficulty. Each irradiated sample was processed chemically and radiomanganese separated from the other activities. The ^{51}Mn activity was determined via (a) decay curve analysis of the 511 KeV γ-ray, (b) growth and decay curve analysis of the 321 KeV γ-ray of ^{51}Cr. The two results agreed within ~ 10%. Preliminary results show that the optimum energy range for the production of ^{51}Mn is $E_d = 9 \rightarrow 5$ MeV. Further work is continuing.

^{55}Co ($T_{1/2}$ = 17.6 h) is a potentially useful radioisotope. As described in the last Progress Report, for its production the $^{54}Fe(d,n)^{55}Co$ process was studied using highly enriched ^{54}Fe as target material. The data analysis has been completed [cf. 9]. This method leads to high-purity ^{55}Co and a small cyclotron is adequate (optimum energy range: $E_d = 10 \rightarrow 5$ MeV). The disadvantage of the process is the high cost of the enriched target material.

^{120}I ($T_{1/2}$ = 1.35 h) and ^{124}I ($T_{1/2}$ = 4.15 d) are longer-lived β^+ emitting radioisotopes of iodine. They are of potential interest for labelling biomolecules for diagnostic investigations using PET. The latter radioisotope is also used in therapeutic studies. In connection with the production of ^{120}I, we investigated the $^{122}Te(p,3n)$ and several other competing reactions on highly enriched ^{122}Te over the proton energy range of 6 to 45 MeV (compact cyclotron CV 28 and Injector of COSY). The optimum energy range for the production of 1.35 h ^{120}I was found to be $E_d = 40 \rightarrow 30$ MeV. However, over the same energy range the 53 min ^{120m}I is also formed; its contribution amounts to ~ 30% of the 1.35 h ^{120}I activity. Since the 53 min isomeric state is also a β^+ emitter, the use of 1.35 h ^{120}I in PET studies demands extra care while making decay corrections.

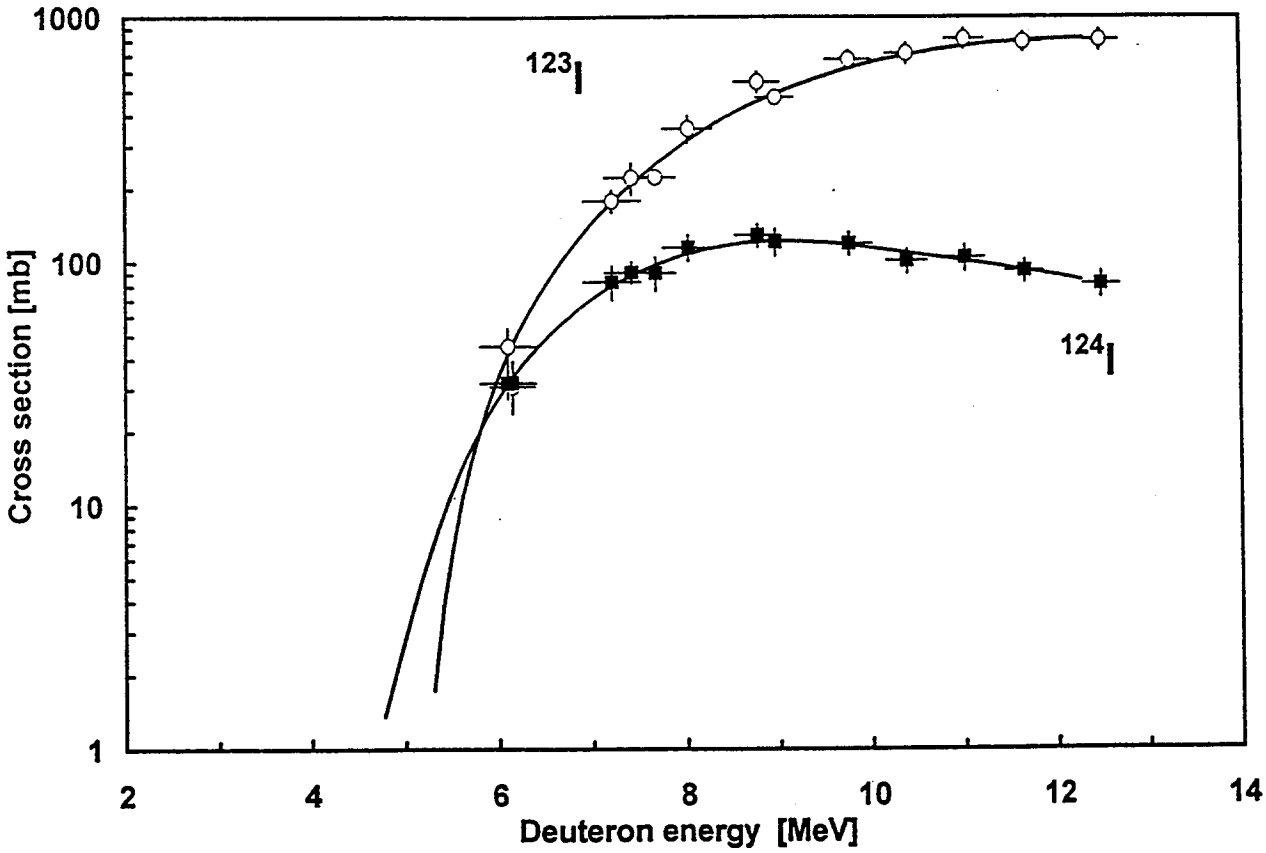

Fig. 3 Excitation functions of $^{123}Te(d,n)^{124}I$ and $^{123}Te(d,2n)^{123}I$ reactions. The solid lines give spline fits to the experimental data (for details cf. Ref. [10]).

^{124}I is generally produced via the $^{124}Te(d,2n)$ and $^{124}Te(p,n)$ processes. Some details on the latter process were given in the last Progress Report. We thought it now worthwhile to investigate the $^{123}Te(d,n)^{124}I$ reaction on enriched ^{123}Te. The results for this and the competing $^{123}Te(d,2n)^{123}I$ reaction are given in Fig. 3. Due to the very close thresholds of the two processes, high-purity ^{124}I is difficult to produce. Since the yield of ^{124}I is also rather low, the method is not to be suggested for production purposes.

Besides the development work on the above mentioned longer-lived β^+ emitters, some optimization studies on the production of ^{15}O ($T_{1/2}$ = 2.0 min), commonly used in PET studies, were also done. Since there is some uncertainty about the levels of the impurities ^{13}N ($T_{1/2}$ = 10 min) and ^{11}C ($T_{1/2}$ = 20.0 min), we measured the excitation functions of the $^{14}N(d,t)^{13}N$ and $^{14}N(d,\alpha)^{11}C$ processes from their respective thresholds up to 14 MeV. At deuteron energies below 8 MeV no impurity was observed.

The nuclear data measurements relevant to the production of the most commonly used SPECT-radioisotope ^{99m}Tc ($T_{1/2}$ = 6.0 h) have the aim to clarify whether this radioisotope can be economically produced at a medium-sized cyclotron. This is a hotly debated issue and the experimental studies have been initiated at the request of the IAEA. A study of the $^{100}Mo(p,2n)^{99m}Tc$ and $^{100}Mo(p,pn)^{99}Mo$ processes on highly enriched ^{100}Mo is envisaged. Irradiations of thin samples have been done with protons of energies up to 65 MeV (Injector of COSY, cyclotron at Louvain-la-Neuve), and presently data analysis is in progress.

The γ-ray emitting radioisotope ^{147}Gd ($T_{1/2}$ = 38.1 h) is well-suited for in-vivo pharmakokinetic investigations on the Gd-complexes used as contrast agents in MRI. As described in the last Progress Report, for its production the $^{147}Sm(^3He,3n)$ and $^{144}Sm(\alpha,n)$ reactions are very suitable. Measurements of excitation functions have been completed [cf. 11] and the $^{147}Sm(^3He,3n)^{147}Gd$ process over the energy range of $E_{^3He}$ = 36 → 13 MeV has been developed to produce sufficient quantities of ^{147}Gd for practical applications.

References

[1] S.M. Qaim, M. Uhl, F. Rösch, F. Szelécsényi: Excitation functions of (p,α) reactions on ^{64}Ni, ^{78}Kr and ^{86}Sr, Phys. Rev. C 52 (1995) 733

[2] S.M. Qaim: Radiochemical studies of complex particle emission in low and intermediate energy reactions, Radiochimica Acta 70,71 (1995) 163

[3] I.-G. Birn, B. Strohmaier, H. Freiesleben, S.M. Qaim: Isomeric cross section ratios for the formation of $^{75m,g}Ge$ in (n,p), (n,α) and (n,2n) reactions from 6 to 15 MeV, Phys. Rev. C 52 (1995) 2546

[4] A. Fessler, S.M. Qaim: Formation of high spin isomers ^{52m}Fe and ^{53m}Fe in ^3He-particle induced nuclear reactions on ^{52}Cr, Radiochimica Acta 72 (1996) 121

[5] S. Sudár, S.M. Qaim: Isomeric cross section ratios for the formation of $^{58m,g}Co$ in neutron, proton, deuteron and α-particle induced reactions in the energy region up to 25 MeV, Phys. Rev. C, in press

[6] S.M. Qaim, F. Cserpák, J. Csikai: Excitation functions of $^{109}Ag(n,2n)^{108m}Ag$, $^{151}Eu(n,2n)^{150m}Eu$ and $^{159}Tb(n,2n)^{158}Tb$ reactions from threshold to 15 MeV, Appl. Radiat. Isotopes 47 (1996) 569

[7] S.M. Qaim, St. Spellerberg, F. Cserpák, J. Csikai: Radiochemical measurement of excitation function of $^{63}Cu(n,p)^{63}Ni$ reaction from 7.2 to 14.6 MeV, Radiochimica Acta, in press

[8] S. Tákács, F. Tárkányi, S.M. Qaim: Excitation function of $^{22}Ne(p,n)^{22}Na$ reaction: possibility of production of ^{22}Na at a small cyclotron, Appl. Radiat. Isotopes 47 (1996) 303

[9] M.R. Zaman, S.M. Qaim: Excitation functions of (d,n) and (d,α) reactions on ^{54}Fe: relevance to the production of high purity ^{55}Co at a small cyclotron, Radiochimica Acta, in press

[10] B. Scholten, S. Tákács, Z. Kovács, F. Tárkányi, S.M. Qaim: Excitation functions of deuteron induced reactions on ^{123}Te: relevance to the production of ^{123}I and ^{124}I at low and medium sized cyclotrons, Appl. Radiat. Isotopes, in press

[11] F.-O. Denzler, F. Rösch, S.M. Qaim: Excitation functions of α- and ^{3}He-particle induced nuclear reactions on highly enriched ^{144}Sm and ^{147}Sm: comparative evaluation of production routes for ^{147}Gd, Radiochimica Acta 69 (1995) 209

INSTITUT FÜR KERN- UND TEILCHENPHYSIK TECHNISCHE UNIVERSITÄT DRESDEN

1. Iron Benchmark Experiments Analysed with the Fusion Evaluated Nuclear Data Library (FENDL)

H. Freiesleben, W. Hansen, D. Richter, K. Seidel, S. Unholzer

Measurements of spectral neutron and photon fluxes from several iron and steel (SS316) assemblies irradiated with 14 MeV neutrons were described in previous progress reports. The analysis of the experimental results, which are sensitive to shield penetration problems of fusion reactor designs, on the basis of nuclear data from the European Fusion File, versions EFF-1 and EFF-2, was also presented. During the last year FENDL files [1] were included in the data testing. FENDL acts as reference library for the design of the International Thermonuclear Experimental Reactor and, therefore, it was extensively tested by an International Working Group [2]. The results of the group, among them the TUD contribution, were discussed at an IAEA Advisory Group Meeting [3].

The geometry of the Fe benchmarks analysed is outlined in Fig. 1. Besides the solid slab two assemblies with a gap (width b = 5.0 cm at position x = 10 cm and 20 cm, respectively) were included in the programme to investigate streaming.

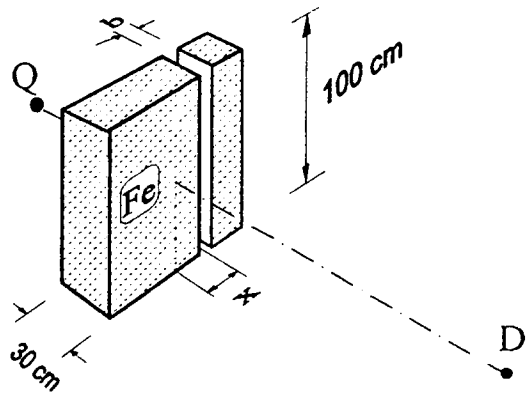

Fig. 1 Benchmark geometry (Q -position of the 14 MeV neutron source, D - detector position)

The spectral neutron and photon fluxes were calculated with the three-dimensional Monte Carlo code MCNP [4]. Detector collimator, walls, floor, assembly racks, air in the experimental hall, source-target backing etc. were taken into account, as well as the neutron detector efficiency in the case of time-of-arrival spectra, such that the calculated fluxes could be directly compared with the measured fluxes (Fig. 2 and Table 1).

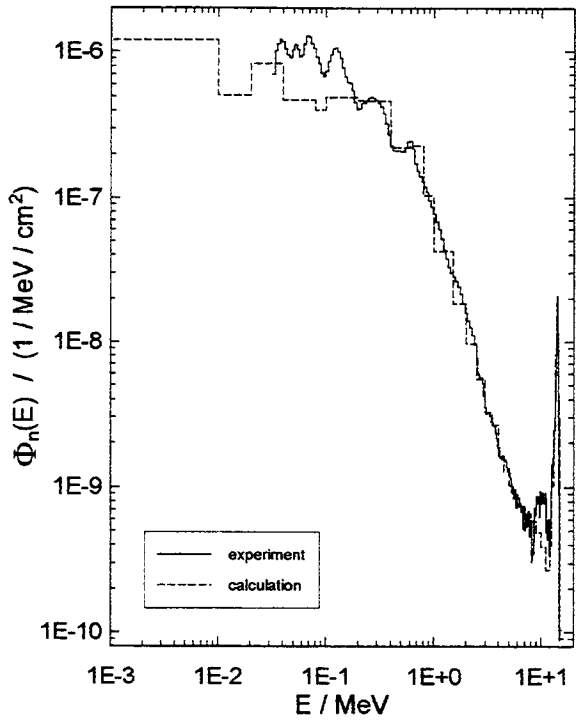

a) low-energy part

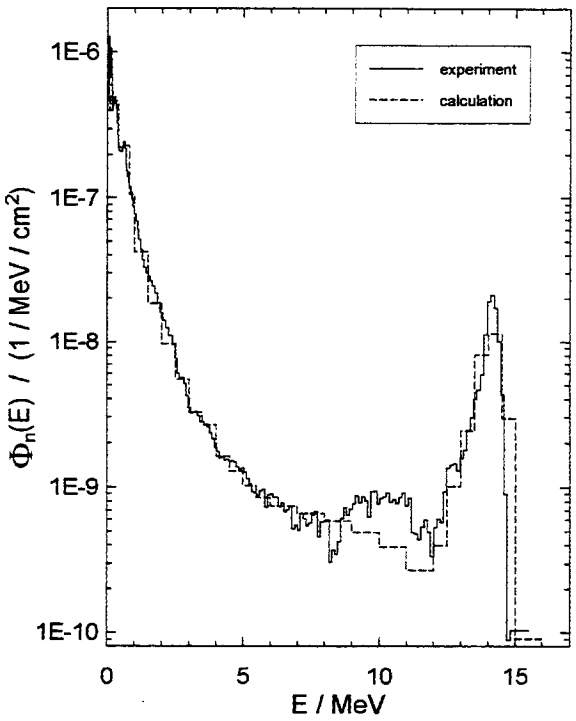

b) high-energy part of the neutron spectrum

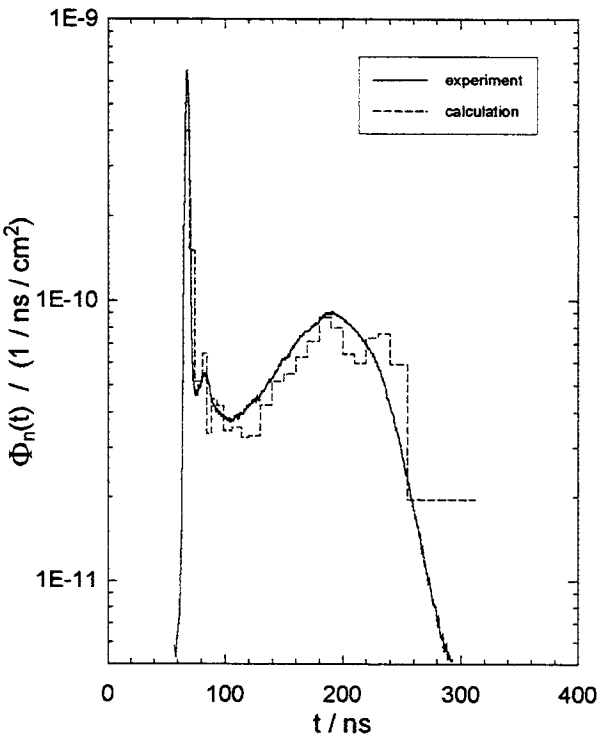

c) neutron time-of-arrival spectrum

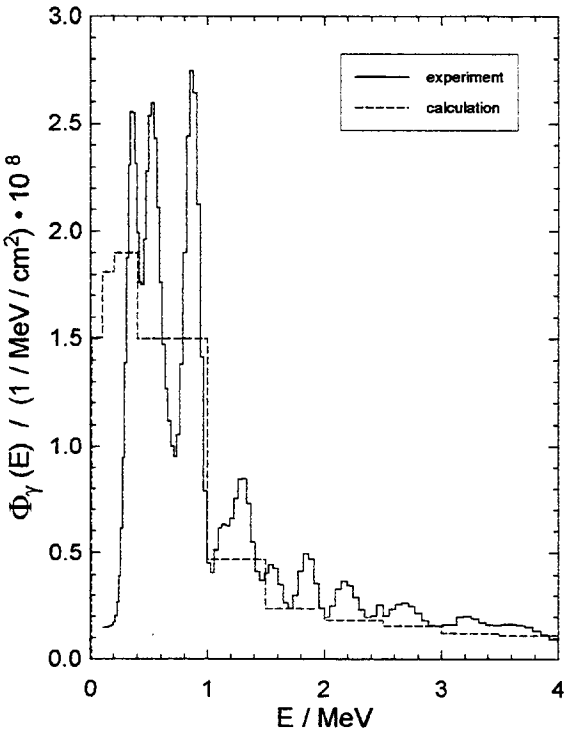

d) photon spectrum up to 4 MeV

Fig. 2 Measured and calculated spectral fluences per one source neutron from the solid slab

Tab. 1 Ratio of calculated to experimental flux from the solid slab (0/0) and from the assembly with a gap (width/position in cm) 5/20 and 5/10

E_n / MeV	0/0	5/20	5/10
0.04 - 1.0	0.88 ± 0.10	0.78 ± 0.09	0.86 ± 0.10
1.0 - 5.0	0.94 ± 0.03	0.80 ± 0.02	0.83 ± 0.02
5.0 - 10.0	1.00 ± 0.07	0.97 ± 0.02	1.00 ± 0.03
10.0 - 15.0	0.87 ± 0.04	0.88 ± 0.02	0.98 ± 0.02
t_n / ns	0/0	5/20	5/10
0 - 81	0.84 ± 0.02	0.86 ± 0.02	0.94 ± 0.02
81 - 200	0.90 ± 0.07	0.90 ± 0.07	0.89 ± 0.07
E_γ / MeV	0/0	5/20	5/10
0.2 - 8.0	0.76 ± 0.02	0.80 ± 0.01	0.86 ± 0.01

The general agreement of experimental and calculated results is good and shows a similar behaviour as obtained with EFF-2 data (Progress Report 1994/95). Compared to EFF-1 calculations the high-energy region of the neutron flux (as well as the flux in the corresponding time-of-arrival interval) and the photon flux in the whole range of measurement are significantly better described by inclusion of pre-compound processes with double-differential cross sections. The remaining underestimations of the experimental results by FENDL data, especially for neutron energies $E < 5$ MeV and between 10 MeV and 15 MeV and for the photon flux, are considerably reduced if resonance fluctuation corrections [5] based on high-resolution measurements at Geel [6] are implemented in the total, the elastic and the inelastic cross sections, as shown by the Petten group [7].

References:

[1] S. Ganesan and P. McLaughlin, FENDL/E - Evaluated Nuclear Data Library of Neutron Interaction Cross-sections and Photon Production Cross-sections and Photon-atom Interaction Cross-sections for Fusion Applications, Version 1.0; Report International Atomic Energy Agency, IAEA-NDS-128 (May 1994)

[2] A. B. Pashchenko, IAEA Consultants' Meeting on Benchmark Validation of FENDL-1, Karlsruhe (Germany), Oct 17-19, 1995; Summary Report INDC(NDS)-351, IAEA Vienna 1996

[3] U. Fischer (ed.), Summary Report of the International Working Group on "Experimental and Calculational Benchmarks on Fusion Neutronics for FENDL Validation", IAEA Advisory Group Meeting on "Completion of FENDL-1 and Start of FENDL-2", Del Mar (USA), Dec. 5-9, 1996

[4] J. F. Briesmeister (ed.), MCNP - a General Monte Carlo N-Particle Transport Code, Version 4A, Report Los Alamos National Laboratory, LA-12625-M (Nov. 1993)

[5] F. H. Fröhner, On Uncertainty Evaluation and Fluctuations in the Resolved and Unresolved Resonance Region, Int. Conf. on Nuclear Data for Science and Technology, Gatlinburg (USA), May 9-13, 1994, Proc. p. 597

[6] K. Berthold, C. Nazareth, G. Rohr, H. Weigmann, Very High Resolution Measurements of the Total Cross Section of Natural Iron, Int. Conf. on Nuclear Data for Science and Technology, Gatlinburg (USA), May 9-13, 1994, Proc. p. 218

[7] A. Hogenbirk, A. J. Koning, H. Gruppelaar, Validation of the EFF-3.0 Evaluation for ^{56}Fe, Report ECN Petten, ECN-R-95-019 (July 1995)

2. Measurement of Spectral Neutron and Photon Fluxes in an ITER Blanket Mock-Up

H. Freiesleben, W. Hansen, D. Richter, K. Seidel, S. Unholzer

Nuclear data libraries are checked by benchmark arrangements which are optimized in geometry and material composition in such a way that nuclear data of selected elemental materials can be investigated separately. Nuclear processes of special interest are enhanced in order to assess the quality of nuclear data libraries. Examples are the Fe and SS316 benchmark experiments described in preceding annual reports [1,2]. In the present Engineering Design Activities for the International Thermonuclear Experimental Reactor (ITER) the experimental validation of the nuclear performance of the ITER shielding system is one of the tasks. Therefore, a mock-up at the Frascati Neutron Generator (FNG) was realized which simulates as close as possible the ITER inboard shield including first wall, blanket, vacuum vessel and toroidal field coils [3]. These bulk shield experiments are performed and analyzed in collaboration by several European and Russian groups. The experimental programme started with measurements of spectral neutron and photon fluxes by the group of TU Dresden because the fluxes are the basic weighing function for the integral quantities to be determined (such as reaction rates or nuclear heating). Because transport codes are well established these experiments represent a test of nuclear data for the calculation of a complex shield configuration.

The bulk shield blanket assembly is outlined in Fig. 1. It consists of a combination of slabs made from Perspex (2 cm thickness each) and SS316 (about 5 cm thickness each) and has a front area of 100 x 100 cm². The total thickness of the assembly is 97 cm including a 1 cm thick Cu layer in front. A central horizontal channel with a diameter of 3 cm enables small detectors to be inserted and was closed by plugs in the experiments described here. Behind this assembly a block of Cu and SS316 plates is arranged simulating the coils for the toroidal magnetic field (dimensions: depth 30 cm, area 47 x 47 cm²). The rear part of the assembly is surrounded with a polythene shield covering also the last 30 cm of the Perspex/SS316 block in order to reduce room-return background.

Neutron spectra were measured in the mock-up in the centre of the assembly (i.e. at the place of the central horizontal channel) at two depths of penetration:

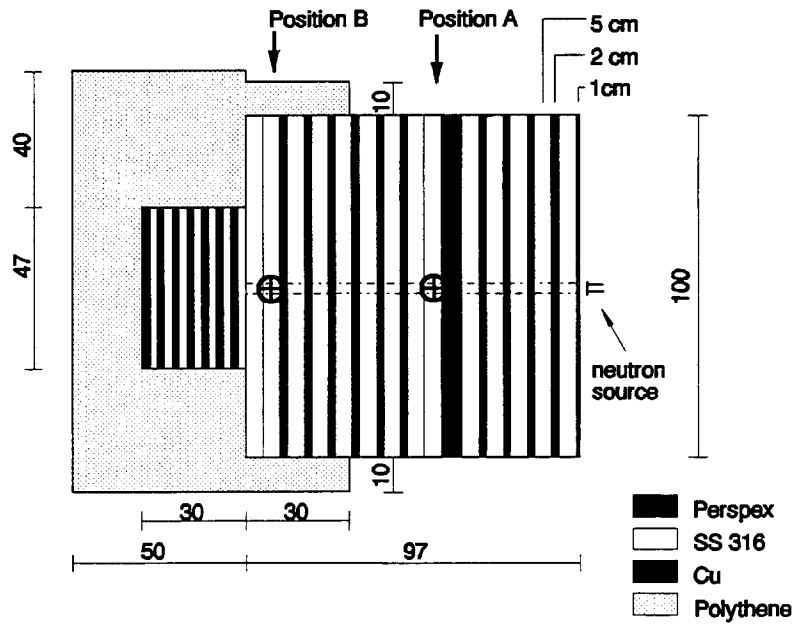

Fig. 1 Bulk shield assembly and positions for neutron energy spectra measurements

Position A:
Measurement inside the first SS316 slab behind the 6 cm thick Perspex layer (total depth 42.5 cm from the front of the assembly). This position characterizes the reverse side of the shield blanket.

Position B:
Measurement in the next to last SS316 layer (total depth 89.5 cm from the front). This position corresponds to the boundary of the vacuum vessel with the coils.

The detectors were inserted into a horizontal rectangular channel in the assembly arranged perpendicular to its axis (cross section 5.0 x 5.5 cm^2), the remaining volume around the detectors was filled with SS316 form bricks.
The FNG neutron source is positioned in a large hall (11.5 x 12.0 x 9.5 m^3); its target is 4 m above the floor. Further actual FNG parameters are: D^+ current at the target up to 1 mA (energy 230 keV) resulting in a maximum neutron source strength of $5 \cdot 10^{10}$ n/s during the experiments.

The neutron energy spectra $\Phi(E)$ were measured in the range between about 20 keV (position A) or 60 keV (position B) and 15 MeV. Gas-filled proportional counters and a stilbene scintillation spectrometer were applied for the measurements in the range up to 3 MeV and a NE213 scintillation spectrometer was used between about 1 MeV and 15 MeV. The spectra were determined on an absolute scale as fluences per one source neutron. Parameters of all detectors are given in Tab. 1. The NE213 scintillation spectrometer was also used for the simultaneous measurement of photon flux spectra by the procedure described in [4].
In order to minimize the interference of the NE213 detector system with the radiation field inside the assembly the photomultiplier was coupled to the scintillator by means of a 50 cm long light guide. By this way, only the scintillator and the light guide have to be inserted into the shield blanket whereas the photomultiplier is outside of the slabs on their surface. The proportional counters with their preamplifiers as well as the stilbene scintillator with its photomultiplier are combined each in housings of 45 mm outer diameter and could be inserted completely into the experimental channels.

Tab. 1 Parameters of the detectors used for the spectral flux measurements

Type	Detector material	Pressure / kPa	Length / cm	Radius / cm	Energy Range / MeV
SP9	H_2	100	-	1.6	0.02 - 0.22
SP2	H_2	400	-	2.0	0.10 - 0.64
NOK1043	H_2	1000	-	2.0	0.30 - 1.05
CHM-49	95%CH_4+5%N_2	400	10	1.55	0.40 - 1.20
Scintillation	Stilbene	-	1.0	0.5	0.70 - 3.0
Scintillation	NE 213	-	3.81	1.91	n: 1.00 - 15.0 γ: 0.20 - 8.0

The satisfying neutron fluence in position A did allow the application of biparametric pulse shape discrimination in the proton recoil counter measurements (detector SP9) such that the energy range could be extended downwards to 20 keV. Pulses are aquired in a biparametric field (energy and pulse rise time) as presented in Fig. 2. Because the pulse rise times of recoil protons (generated by neutrons) and electrons (generated by photons in the counter wall) overlap each other they cannot be simply discriminated by a threshold. The photon background must be determined in a separate measurement and substracted after appropriate normalization.

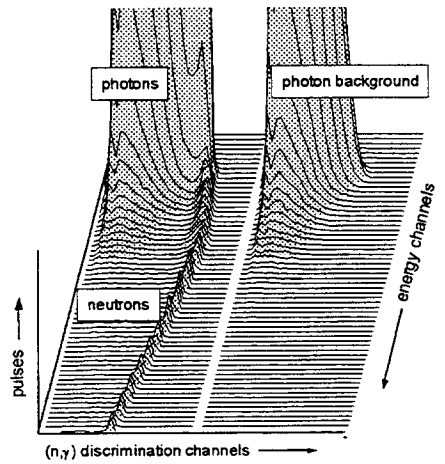

Fig. 2 Biparametric measurement with electronic pulse shape discrimination for proton recoil counters

Preliminary evaluations of the measured neutron spectra are compared to calculations in Fig. 3 (position A) and Fig. 4 (position B). The calculations were performed by means of the Monte-Carlo code MCNP-4A [5] and nuclear data from the ITER reference library FENDL-1 [6]. A final evaluation of measured spectra and a detailed analysis of experimental and calculational results is in progress.

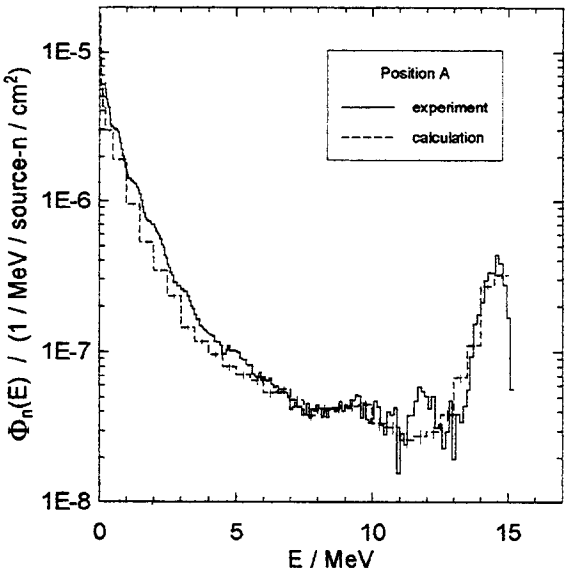

Fig. 3 Measured neutron spectrum in position A compared to calculation (FENDL-1 data)

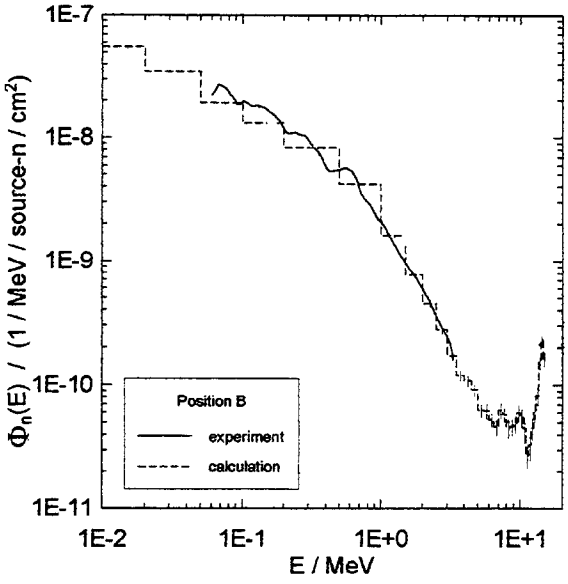

Fig. 4 Measured neutron spectrum in position B compared to calculation (FENDL-1 data)

The work was supported by the European Fusion Technology Programme ITER Task T218.

References:

[1] H. Freiesleben, W. Hansen, D. Richter, K. Seidel, S. Unholzer, Benchmarks of Iron Nuclear Data, Progress Report on Nuclear Data Research in the Federal Republic of Germany, ed. by S.M. Qaim, NEA/NSC/DOC(94)21, 1994

[2] H. Freiesleben, W. Hansen, D. Richter, K. Seidel, S. Unholzer, Benchmarks of SS316 Nuclear Data, Progress Report on Nuclear Data Research in the Federal Republic of Germany, ed. by S.M. Qaim, NEA/NSC/DOC(95)10, INDC(Ger)-040, Jül-3086, July 1995

[3] P. Batistoni et al., 1st Intermediate Report on Pre-Analysis of Experiments, ITER Task T218, Shielding Neutronics Experiments, Subtask A/EU Contribution, ENEA C.R. Frascati, Fusion Division, Neutronics Section, Dec. 1995

[4] H. Freiesleben, W. Hansen, H. Klein, T. Novotny, D. Richter, R. Schwierz, K. Seidel, M. Tichy and S. Unholzer, Experimental Results of an Iron Slab Benchmark, Report TU Dresden, TUD-PHY-94/2, Febr. 95

[5] J. F. Briesmeister (ed.), MCNP - a General Monte Carlo N-Particle Transport Code, Version 4A, Report Los Alamos National Laboratory, LA-12625-M (Nov. 1993)

[6] S. Ganesan and P. McLaughlin, FENDL/E - Evaluated Nuclear Data Library of Neutron Interaction Cross-sections and Photon Production Cross-sections and Photon-atom Interaction Cross-sections for Fusion Applications, Version 1.0; Report International Atomic Energy Agency, IAEA-NDS-128 (May 1994)

3. Kβ/Kα Intensity Ratios and Chemical Effects of 3d Elements

L. Rebohle, U.Lehnert, G. Zschornack

It is well known that the Kβ/Kα intensity ratio of 3d elements is influenced by the chemical binding. The difference between various compounds can easily reach a value of 10 % and more. Due to the importance of the Kβ/Kα intensity ratio for elemental analysis and many other subjects a lot of investigations have been done in the past [1 - 7] . Theoretical values for pure elements were calculated by Scofield [8] as well as Jankowski and Polasik [9].

In this work we have measured the Kβ/Kα intensity ratio for several compounds of 3d elements as a function of the formal oxidation number. Two different kinds of samples were used in the experiment. In some cases metallic foils with a thickness of about 100 µm were available, whereas the other compounds to be examined were pressed into disks with a diameter of 20 mm and a thickness varying between 3 mm and 10 mm. The specimen powder was mixed with polyvinyl alcohol C_2H_4O as an organic binder. Thereby, the mass fraction of the specimen powder was between 10 % and 50 %.

A commercial X-ray tube with a known spectrum was used to produce K-vacancies. The X-ray beam passed a 1 mm thick aluminium plate which cuts off the energy spectrum of the tube below 10 keV (0.1 % transmission). After passing 6 cm of air the beam enters a vacuum chamber through a beryllium window and hits the target surface at a 45° angle, whereas the characteristic radiation was detected at an angle of 90° with respect to the primary beam. For these measurements a Si(Li)-detector with a resolution of 145 eV for Fe Kα X-rays was used.

The peak area of a Kα or Kβ line with contents of 10^5 to 10^7 counts was obtained by optimizing a model function $s(x)$, describing the measured spectrum. It can be expressed as

$$s(x) = \left(b(x) + \sum_{i=1}^{N} p_i(x) \right) \cdot \prod_{j=1}^{M} a_i(x) \,, \qquad (1)$$

where $b(x)$ is the background model., the $p_i(x)$ are single peaks and the $a_i(x)$ absorbtion edges. The peaks are represented by the sum of a Voigt function [10] with a tail. To get the best parameter set we used a least-squares fit procedure based on an evolutionary algorithm (cf. Ref. [11]). If we take the chi-square function at a fixed value, we define a confidence region boundary in the parameter space around the global minimum. The range of the confidence region containing the "true" parameter set with a probability of 68.3 % results in the uncertainty of our fit. Details of the spectra evaluation are given in Ref. [12].

The Kβ/Kα intensity ratios f_M obtained from the spectra evaluation must be corrected to get the original intensity ratios f_0 :

$$f_0 = C_e C_m C_b f_M \qquad (2)$$

Thereby, the corrections C_e , C_m *and* C_b are related to detector efficiency, matrix effects and background radiation. It is neccessary to note, that only a careful analysis of the contributions to eq . 2 allows realistic error estimations. Thus, the small errors shown in Fig. 1 for values presented by different authors may arise from underestimations of the correction factors in eq. 2.

Table 1 gives a summary of the measured Kβ/Kα intensity ratios and their uncertainties. At a given Z the Kβ/Kα intensity ratio shows the tendency to rise with increasing formal oxidation number, like it can be well observed from the values of Ti, Co, Ni and Cu. The dependence for V, Cr, Fe and Mn is more complex due to the fact, that the Kβ/Kα intensity ratio is affected by the chemical bonding type and the individual features of the molecular structure too.

The Kβ/Kα intensity ratios of different compounds and from different studies are shown in Fig.1.

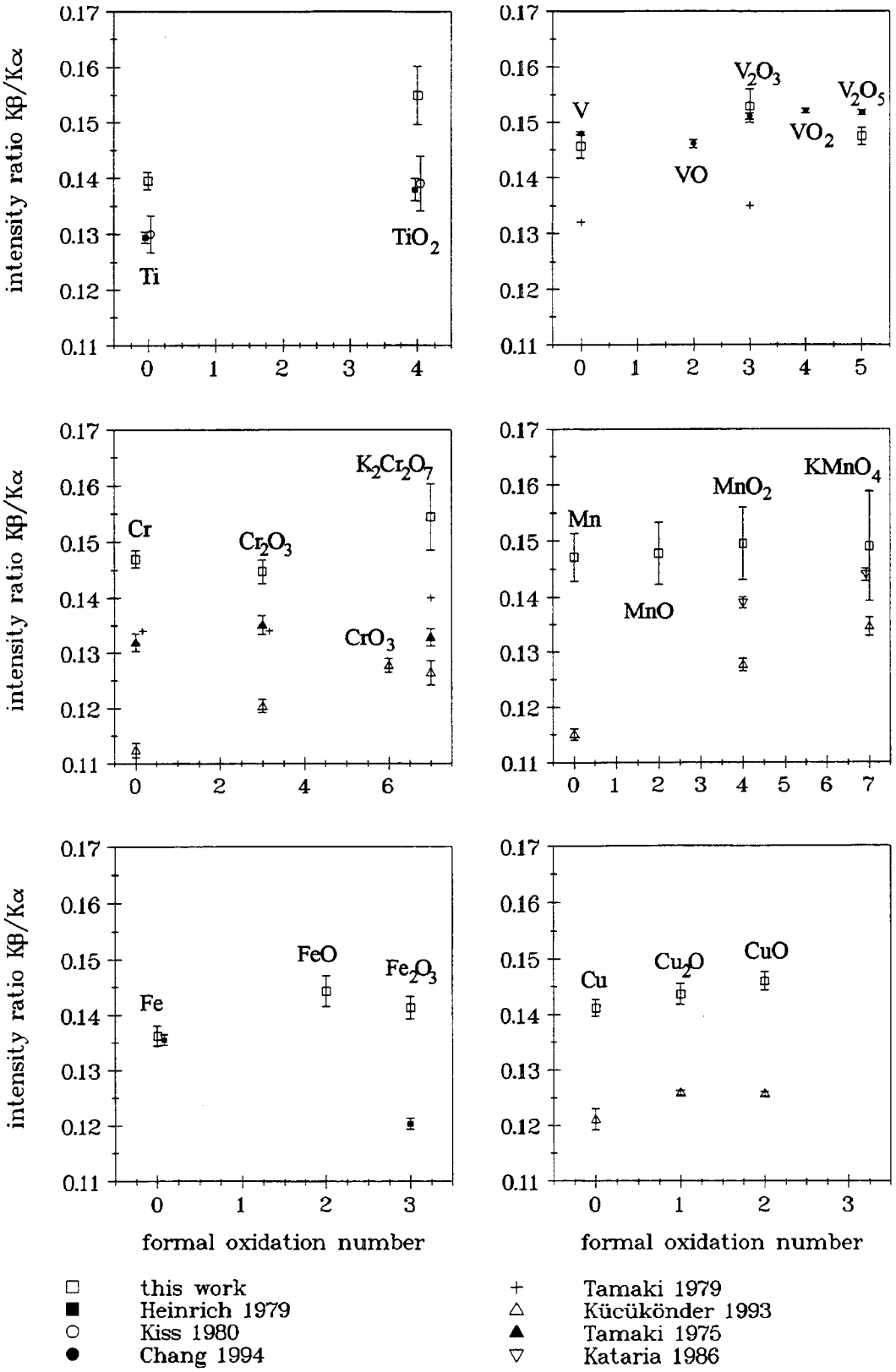

Fig. 1 The measured Kβ/Kα intensity ratios in comparison with other studies [1, 2, 6, 7, 13, 14, 16]. They show the tendency to increase with increasing formal oxidation number. But the uncertainties of the measured values don't allow any other statement about the specific dependence of the Kβ/Kα intensity ratio.

The uncertainties of the measured values are in some cases too large to allow any statement about the specific dependence of the Kβ/Kα intensity ratio from the formal oxidation number.

A correlation between the Kβ/Kα intensity ratio of 3d-elements and the chemical state was found in this work. Excluding the values of Sc, Mn and Zn we can state the tendency of the Kβ/Kα intensity ratio to rise with increasing formal oxidation number. Except the demand for a higher precision in future experiments it is planned to investigate the dependence of the Kβ/Kα intensity ratio on kind and thickness of the samples and to improve the model describing the measured spectra.

The work has been supported by BMBF under contract No. 06 DD 111. We want to thank all colleagues of the *Physikalisch-Technische Bundesanstalt Braunschweig, Germany* who supported us to calibrate the detector, especially Dr. Dangendorf and Dr. Janßen.

Tab. 1 Measured Kβ/Kα intensity ratios. The uncertainties are both statistical and systematic.

compound	intensity ratio	compound	intensity ratio
S_2O_3	0.1467 ± 0.0014	Fe	0.1362 ± 0.0018
Ti	0.1395 ± 0.0016	$FeSO_4$	0.1478 ± 0.0026
TiO_2	0.1549 ± 0.0052	FeO	0.1442 ± 0.0027
V	0.1456 ± 0.0021	Fe_2O_3	0.1413 ± 0.0020
V_2O_3	0.1529 ± 0.0031	Co	0.1400 ± 0.0022
V_2O_5	0.1474 ± 0.0016	$CoCl_2$	0.1445 ± 0.0024
Cr	0.1469 ± 0.0016	CoO	0.1450 ± 0.0027
Cr_2O_3	0.1447 ± 0.0021	Ni	0.1403 ± 0.0015
$K_2Cr_2O_7$	0.1544 ± 0.0059	NiO	0.1450 ± 0.0015
Mn	0.1471 ± 0.0042	Cu	0.1412 ± 0.0016
$MnSO_4$	0.1436 ± 0.0070	Cu_2O	0.1436 ± 0.0018
MnO	0.1478 ± 0.0055	CuO	0.1459 ± 0.0016
MnO_2	0.1495 ± 0.0065	Zn	0.1528 ± 0.0017
$KMnO_4$	0.1490 ± 0.0098	ZnO	0.1487 ± 0.0015

References

[1] Y. Tamaki, T. Omori, T. Shiokawa, Radiochem. Radioanal. Lett. 20 (1975) 255
[2] Y. Tamaki, T. Omori, T. Shiokawa, Radiochem. Radioanal. Lett. 37 (1979) 39
[3] G. Brunner, M. Nagel, E. Hartmann, E. Arndt, J. Phys. B: At. Mol. Phys. 15 (1982) 4517
[4] T. Mukoyama, K. Taniguchi, H. Adachi, Phys. Rev. B 34 (1986) 3710
[5] K. Taniguchi, T. Mukoyama, H. Adachi, J. Physique C 9 (1987) 757
[6] A. Küçükönder, Y. Şahin, E. Büyükkasap, A. Kopya, J. Phys. B: At. Mol. Phys. 26 (1993) 101
[7] C. Chang et al. , J. Phys. B: At. Mol. Phys. 27 (1994) 5251
[8] J.H. Scofield, Phys. Rev. A 9 (1974) 1041
[9] K. Jankowski, M. Polasik, J. Phys. B: At. Mol. Phys. 22 (1989) 2369
[10] B.H. Armstrong, J. Quant. Spectrosc. Radiat. Transfer. 7 (1967) 61
[11] D. Küchler, U. Lehnert, G. Zschornack, Nuclear Instruments & Methods, B103 (1995) 243
[12] L. Rebohle; Diploma Thesis, Institut für Kern- und Teilchenphysik, TU Dresden, Dresden, 1995
[13] K. Kiss, J. Pálinkás, B. Schlenk, Radiochem. Radioanal. Lett. 45-3 (1980) 213
[14] K.F.J. Heinrich, C.E. Fiori, R.L. Myklebust, J. Appl. Phys. 50 (1979) 5589
[15] C.V. Raghavaiah et al. , X-ray Spectrom. 21 (1992) 239
[16] S.K. Kataria, R. Govil,A. Saxena, X-ray Spectrom. 15 (1986) 49

ABTEILUNG NUKLEARCHEMIE
UNIVERSITÄT ZU KÖLN
AND
ZENTRUM FÜR STRAHLENSCHUTZ UND RADIOÖKOLOGIE
UNIVERSITÄT HANNOVER

1. An Experimental Data Base of Thin-Target Cross Sections for Residual Nuclide Production by Proton-Induced Reactions on Twenty Target Elements Ranging from Carbon to Gold

R. Michel[1], R. Bodemann[1], H. Busemann[1], R. Daunke[1], M. Gloris[1], B. Klug[1], A. Krins[1], H.-J. Lange[1], I. Leya[1], M. Lüpke[1], S. Neumann[1], H. Reinhardt[1], M. Schnatz-Büttgen[1], U. Herpers[2], Th. Schiekel[2], F. Sudbrock[2], B. Holmqvist[3], H. Condé[4], P. Malmborg[5], M. Suter[6], B. Dittrich-Hannen[6], P.-W. Kubik[7], H.-A. Synal[7]

A wide variety of applications (e.g. accelerator-based nuclear waste transmutation and energy amplification, medical therapy, interactions of cosmic ray particles with matter, accelerator and space technology) is strongly dependent on reliable nuclear data at medium energies [1]. These data needs cover - but are by no means limited to - data for nuclear reactions induced by neutrons and protons with energies of up to several GeV.

An application of medium-energy nuclear data which is particularly well developed is the modelling of cosmogenic nuclide production rates. Cosmogenic nuclides are produced by the interaction of solar and galactic cosmic ray particles with matter. For the interpretation of the observed abundances of cosmogenic nuclides in extraterrestrial matter, such as lunar surface materials, meteorites and cosmic dust, reliable model calculation of production rates is a basic requirement [2]. During recent years, an experimental and theoretical basis was established to calculate cosmogenic nuclide production rates by solar and galactic cosmic ray particles with the required accuracy of better than 10 % for production rates and better than 3 % for production rate ratios; [3] and references therein. These model calculations combine spectra of primary and secondary particles calculated by Monte-Carlo techniques using the HERMES code system [4] with thin-target cross sections of the underlying nuclear reactions induced by primary and secondary protons and by secondary neutrons.

---

1 Zentrum für Strahlenschutz und Radioökologie, Universität Hannover, F.R.G.

2 Abteilung Nuklearchemie, Universität zu Köln, F.R.G.

3 Department of Neutron Research at Studsvik, University of Uppsala, Sweden

4 Department of Neutron Research, University of Uppsala, Sweden

5 The Svedberg Laboratory, University of Uppsala, Sweden

6 Institut für Teilchenphysik, ETH Hönggerberg, Zürich, Switzerland

7 Paul Scherrer Institute c/o Institut für Teilchenphysik, ETH Hönggerberg, Zürich, Switzerland

To provide the necessary reaction data, systematic measurements of cross sections for residual nuclide production by p-induced reactions from thresholds up to 2.6 GeV were performed using accelerators at CERN/Geneve, IPN/Orsay, KFA/Jülich, LANL/Los Alamos, LNS/Saclay, PSI/Villigen, TSL/Uppsala, Université Catholique/Louvain La Neuve. Twenty target elements, namely C, N, O, Mg, Al, Si, Ca, Ti, Mn, Fe, Co, Ni, Cu, Nb, Sr, Y, Zr, Nb, Ba and Au, were investigated. A collaboration of up to 13 institutes at Ahmedabad, Bordeaux, Köln, Hannover, Jülich, Mainz, New Brunswick, Philadelphia, Studsvik, Uppsala and Zürich contributed to these investigations. A considerable amount of nuclear data was published earlier, see [5, 6] and references therein. However, all these publications cover just a minor part of the entire data base, which was completed for these elements last year.

Presently, a report of the still unpublished cross sections for proton-induced reactions and a comprehensive computerized data base of all the results is under preparation [7]. In cooperation with the NEA Nuclear Data Bank of the OECD/Paris the data base will be translated to EXFOR format and will be made available in electronic form. It covers all the above target elements and presents new data from recent experiments at PSI, TSL, CERN, LNS, and LANL. The entire data set covers nearly 550 target/product combinations with about 15,000 cross sections, of which more than 10,000 were not published earlier.

Except for gold, all of the above elements are cosmochemically relevant target elements. Gold was included into our studies for systematic reasons to get some first impression about proton-induced reactions on heavy target elements. As an example, excitation functions for residual nuclide production from gold are shown in Fig. 1 which cover the various reaction modes observable for such high-mass targets. Plots of the cross sections as functions of product mass numbers at various energies clearly exhibit the effect of compound, preeqilibrium, and spallation raections as well as of fragmentation and fission (Fig. 2).

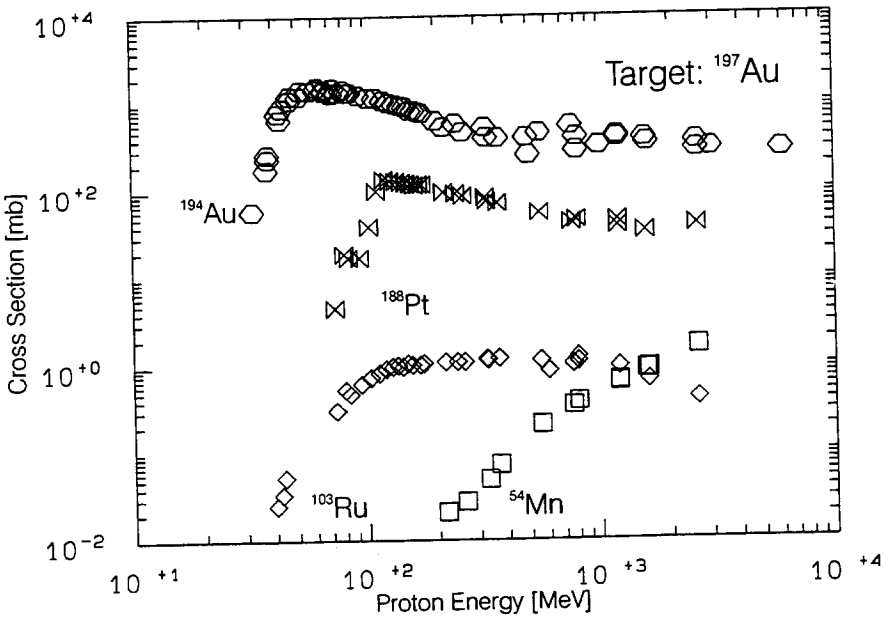

Fig. 1 Experimental excitation functions for the production of ^{54}Mn, ^{103}Ru, ^{188}Pt and ^{194}Au by proton-induced reactions on gold. The data are exclusively from this work.

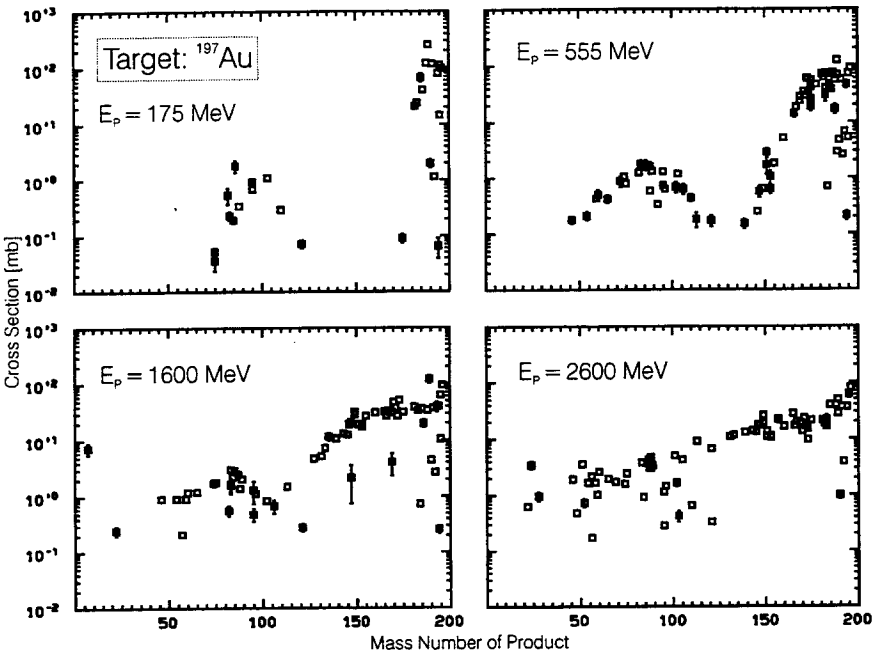

Fig. 2 Experimental cross sections for residual nuclide production by p-induced reactions on gold as function of product mass number. The data are exclusively from this work.

The data needs for such reactions on heavy target elements strongly increased during recent years because of technical applications such as spallation neutron sources and accelerator-based nuclear waste transmutation [8] and energy amplification [9]. Therefore, we have extended our activities to systematic investigations of proton-induced reactions on medium and heavy target elements in order to satisfy some of these data needs (see chapter 3).

Since such experiments are costly and time consuming, it will also be important to rely on nuclear modelling to provide the reaction data needed. In order to evaluate the quality of models and codes when calculating nuclear reaction data, international model and codes intercomparisons were initiated and perfomed by the NEA/NSC. Two exercises were designed to assess the predictive power of current nuclear models in the intermediate energy region for the calculation of thin target double differential cross sections [10] and of transport phenomena in thick targets [11]. A follow-up specialists' meeting [12] recommended that the next step should be a model and code intercomparison aimed at the calculation of isotope yields.

Specifications for an International Codes and Model Intercomparison for Intermediate Energy Activation Yields were published in May 1995 [13]. This third intercomparison is mainly relying on the experimental data base described here. The exercise is not limited to isotopes near the target, but includes a wide range of masses and atomic numbers, so as to test also spallation, fragmentation and heavy cluster emission. The task was to calculate thin-target activation yields for incident protons with energies from thresholds up to 5 GeV with a narrow grid of energy points. Targets were chosen, in order to cover a large mass range and the different types of materials at the same time which are important for a technological application. The target elements oxygen,

aluminum, iron, zirconium and gold with natural isotopic composition were selected. Furthermore, cobalt was selected with some (p,xn)- and (p,pxn)- reactions, in order to test the behaviour of models when calculating nuclide production near closed shells. About 20 participants in the intercomparison provided 29 contributions covering the various targets and the entire energy region as far as this was practical. Presently, the results of the intercomparision are being analyzed and a report is being prepared for publication in 1996.

Acknowledgement The authors thank the authorities of the accelerators for making available the beam-time and the accelerator staffs for their essential cooperation and support. This work was supported partially by the Deutsche Forschungsgemeinschaft, Bonn, and by the CEC in the Human Capital and Mobility Programme.

2. Cross Sections for the Proton-Induced Production of the Cosmogenic Long-lived Radionuclides ^{14}C and ^{36}Cl

F. Sudbrock[1], U. Herpers[1], U. Neupert[2], R. Michel[2], B. Holmqvist[3], H. Condé[4], P. Malmborg[5], H.-A. Synal[6], G. Bonani[7], M. Suter[7]

In order to extend our data base of cross sections for the proton-induced production of long-lived cosmogenic radionuclides, [5, 6, 14 - 16] and references therein, we investigated the production of the radionuclides ^{14}C and ^{36}Cl. The irradiation experiments were carried out at the Svedberg Labaratory/University of Uppsala/ Sweden up to 180 MeV and for higher energies at the Laboratoire National Saturne/Saclay/France. Nine different target elements (Ti, V, Mn, Fe, Ni, Cu, Y, Ag and In) were investigated for the production of ^{36}Cl and two target elements (Fe and Ni) for that of ^{14}C. At Uppsala the stacked-foil technique was used, while at Saclay single energy points were determined in order to minimize the action of secondaries at the higher energies. The proton energies of the individual targets in target stacks were calculated according to the work of Anderson and Ziegler [17]. Proton fluxes were monitored via the reaction $^{27}Al(p,3p3n)^{22}Na$ using the evaluated data of Tobailem and de Lassus St. Genies [18] for energies above 200 MeV and the experimental data by Steyn et al. [19] at lower energies. The chemical procedure for the separation of ^{36}Cl and ^{14}C are described in detail elsewhere [16, 20]. For references and details of the AMS measrements which were done at the PSI/ETH AMS facility in Zürich/Switzerland see [21].

---

1 Abteilung Nuklearchemie, Universität zu Köln, F.R.G.

2 Zentrum für Strahlenschutz und Radioökologie, Universität Hannover, F.R.G.

3 Department of Neutron Research at Studsvik, University of Uppsala, Sweden

4 Department of Neutron Research, University of Uppsala, Sweden

5 The Svedberg Laboratory, University of Uppsala, Sweden

6 Paul Scherrer Institue c/o Institut für Teilchenphysik, ETH Hönggerberg, Zürich, Switzerland

7 Institut für Teilchenphysik, ETH Hönggerberg, Zürich, Switzerland

Here we report the new results which were obtained during the last year (table 1). As an example we show the excitation function for the production of ^{36}Cl from Cu and of ^{14}C from iron and nickel in Fig. 3. The experimental data are compared with theoretical ones calculated by the code HET-KFA2 within the HERMES code system [4]. The high-energy data of ^{36}Cl from Cu are fairly well described contrary to the production of ^{14}C from Fe and Ni which is underestimated by at least a factor of ten. These underestimates point to ^{14}C being rather a fragmentation than a spallation product in these reactions. The HET-KFA2 calculations only represent the production by spallation and do not include fragmentation reactions.

Acknowledgement: The authors thank the staffs of The Svedberg Laboratory/University of Uppsala/Sweden and of Laboratoire National Saturne/Saclay/France for their kind cooperation. This work was supported in part by the Deutsche Forschungsgemeinschaft, Bonn, by the Swedish National Science Research Council, Stockholm, and by the Swiss National Science Foundation, Bern.

Table 1: Experimental cross sections for the production of ^{36}Cl from Ti, V, Mn, Fe, Ni, Cu, Y, Ag, In and of ^{14}C from Fe and Ni.

E [MeV]	ΔE [MeV]	σ [mb]	Δσ [mb]
	^{14}C(Fe)		
280.	1.	0.051	0.004
383.	1.	0.113	0.009
599.	1.	0.332	0.027
800.	1.	0.652	0.052
1200.	1.	1.34	0.11
1600.	1.	1.99	0.16
2600.	1.	2.98	0.24
	^{14}C(Ni)		
275.	1.	0.030	0.003
378.	1.	0.068	0.005
579.	1.	0.138	0.011
800.	1.	0.468	0.037
1200.	1.	1.11	0.09
1590.	1.	1.46	0.12
2600.	1.	1.51	0.12
	^{36}Cl(Ti)		
30.7	1.	11.5	0.5
800.	1.	18.5	0.8
1200:	1.	14.1	0.6
1600.	1.	15.5	0.7
	^{36}Cl(V)		
95.	1.	0.29	0.02
800.	1.	12.3	0.6
1200.	1.	13.3	0.6
1600.	1.	13.8	1.1
2600.	1.	11.0	0.5
	^{36}Cl(Mn)		
800.	1.	9.18	0.413
1600.	1.	14.3	0.121
2600.	1.	11.9	0.535

E [MeV]	ΔE [MeV]	σ [mb]	Δσ [mb]
	^{36}Cl(Fe)		
2600.	1.	10.4	0.5
	^{36}Cl(Ni)		
1600.	1.	9.12	0.80
2600.	1.	8.22	0.41
	^{36}Cl(Cu)		
141.	1.	0.0120	0.0017
158.	1.	0.0370	0.0024
226.	2.	0.0805	0.0052
271.	1.	0.170	0.009
338.	2.	0.392	0.019
374.	1.	0.581	0.026
800.	1.	3.63	0.17
1200.	1.	5.85	0.25
1600.	1.	7.92	0.67
	^{36}Cl(Cu)		
2600.	1.	7.50	0.34
	^{36}Cl(Y)		
772.	1.	0.110	0.061
1160.	1.	3.70	0.20
1560.	1.	11.6	0.59
	^{36}Cl(Ag)		
570.	1.	0.124	0.008
772.	1.	0.126	0.006
	^{36}Cl(In)		
352.	1.	0.97	0.26
568.	1.	0.81	0.16
1180.	1.	0.34	0.24
1580.	1.	0.30	0.24

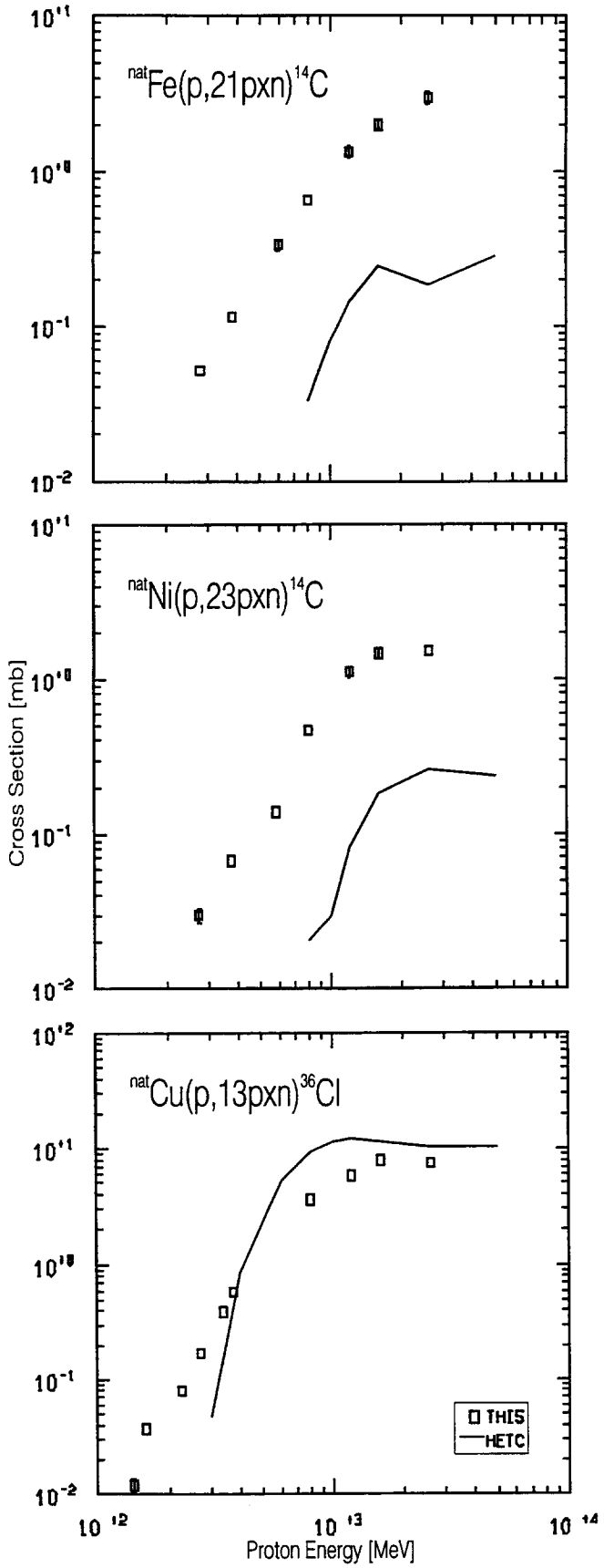

Fig. 3 Experimental and calculated excitation functions for the production of ^{14}C from iron and nickel and of ^{36}Cl from copper.

3. Residual Nuclide Production by Proton-Induced Reactions on Heavy Elements Relevant for Transmutation Techniques

M. Gloris[1], R. Michel[1], U.Herpers[2], F. Sudbrock[2], B. Holmqvist[3], H. Condé[4],P. Malmborg[5]

Transmutation of radioactive waste is presently under investigation as a possibility to reduce the risk potential of long-lived radionuclides. It is intended to transform these nuclei with neutrons of high flux density into short-lived or stable ones. The neutrons are foreseen to be produced in spallation reactions induced by protons of about 1 to 1.5 GeV energy in heavy target elements. For a complete modelling of these processes, a wide variety of hitherto not available nuclear data is needed. In particular, cross sections for p-induced residual nuclide production in possible spallation targets like bismuth, lead or tungsten are needed. Such cross sections are either not available or are sparse, and some existent data are contradictory.

In order to establish a better and more comprehensive data base we carried out irradiation experiments at the accelerators of the Laboratoire National Saturne/Saclay/France and at The Svedberg Laboratory/Uppsala/ Sweden. Relying on our experience based on earlier experiments, e.g. [5,6], we employed the stacked-foil-technique in the experiments at Uppsala, only. At Saclay single energy points were determined in order to minimize the action of secondaries at the higher energies. Besides target elements relevant for transmutation techniques more targets were included to satisfy other needs covering a broad range of masses. Cross sections were determined by γ-spectrometry and accelerator mass spectrometry. For experimental details see [22].

The experiments are still going on. But as illustrative example we show in Fig. 4 some results for the target element Pb. Product masses span a wide range and quite different excitation functions are obtained. Three typical reaction types can be distinguished: direct or preequlibrium-dominated reactions (^{205}Bi), spallation reactions (^{175}Hf) and fission reactions with high thresholds (^{103}Ru) and with relatively low thresholds (^{83}Rb). For a detailed discussion see [22, 23]-

Up to now, we have nearly completed the evaluation of the irradiations of the thin lead targets resulting in excitation functions for more than 70 radionuclides in an energy range from 60 MeV up to 2.6 GeV. The first results from Bi-targets will be presented shortly [22]. Other target elements, such as W, Ta, Ir, and Re, are irradiated and measured. Due to the complexity of the γ-spectra obtained, the evaluation will take more time than originally expected. Further irradiations are planned at the Paul Scherrer Institute/Villigen/Switzerland to extend our knowledge down to threshold energies of all measured product nuclides.

---

1 Zentrum für Strahlenschutz und Radioökologie, Universität Hannover, F.R.G.

2 Abteilung Nuklearchemie, Universität zu Köln, F.R.G.

3 Department of Neutron Research at Studsvik, University of Uppsala, Sweden

4 Department of Neutron Research, University of Uppsala, Sweden

5 The Svedberg Laboratory, University of Uppsala, Sweden

Acknowledgement The authors thank the authorities of LNS and TSL for the beam-time and the accelerator staffs for their careful cooperation and support. This work was supported partially by the Deutsche Forschungsgemeinschaft, Bonn, and by the CEC in the Human Capital and Mobility Programme.

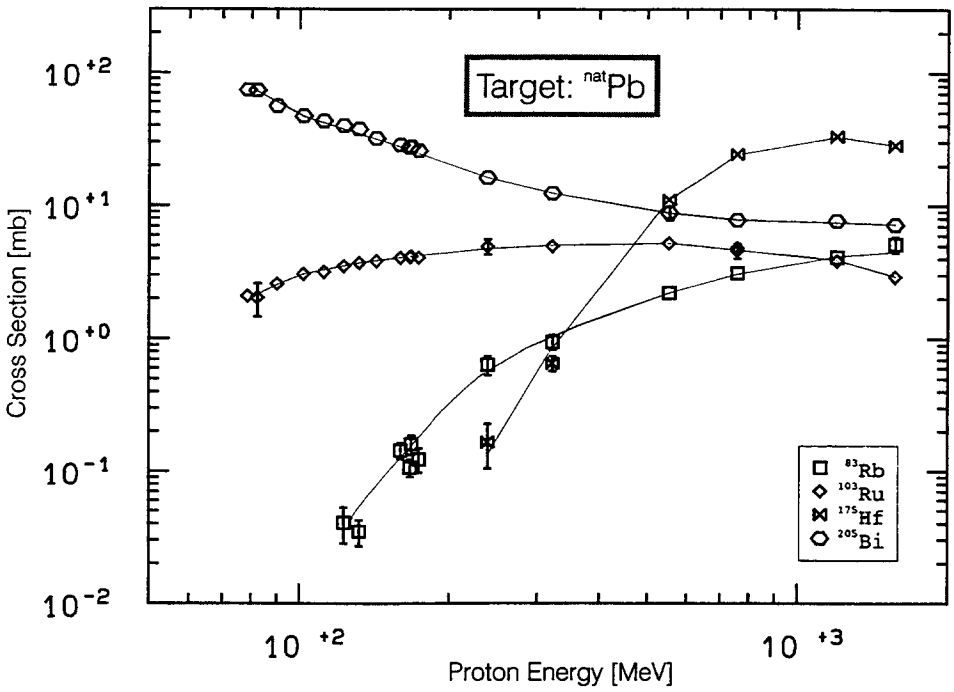

Fig.4 Experimental excitation functions for the proton-induced production of ^{83}Rb, ^{103}Ru, ^{175}Hf, and ^{205}Bi in lead of natural composition; full lines are eye-guides only.

References

[1] N.P. Kocherov, ed., Intermediate Energy Nuclear Data for Applications, INDC(NDS)-245, IAEA, Wien.

[2] R. Michel, Nuclear Data for the Interpretation of Cosmic Ray Interactions with Matter, Nuclear Data for Science and Technology, J.K. Dickens (ed.), pp. 337 - 343 (1994) American Nuclear Society, La Grange Park, Illinois.

[3] R. Michel, L. Borges, I. Leya, Production of Cosmogenic Nuclides in Meteoroids - Accelerator Experiments and Model Calculations to Decipher the Cosmic Ray Record in Extraterrestrial Matter, Proceedings ecaart 4, Nucl. Instr. Meth. Phys. Res. B (1996) in press.

[4] P. Cloth, D. Filges, R.D. Neef, G. Sterzenbach, Ch. Reul, T.W. Armstrong, B.L. Colborn, B. Anders, H. Brueckmann, HERMES High Energy Radiation Monte Carlo Elaborate System, Juel-2203 (1988).

[5] R. Michel, M. Gloris, H.-J. Lange, I. Leya, M. Lüpke, U. Herpers, B. Dittrich-Hannen, R. Rösel, Th. Schiekel, D. Filges, P. Dragovitsch, M. Suter, H.-J. Hofmann, W. Wölfli, P.W. Kubik, H. Baur, R. Wieler, Production of Radionuclides from Target Elements (Z < 29) by Proton-Induced Reactions between 800 and 2600 MeV, Nucl. Instr. Meth. Phys. Res. B 103 (1995) 183 - 222.

[6] T. Schiekel, U. Herpers, M. Gloris, I. Leya, R. Michel, B. Dittrich-Hannen, H.-A. Synal, M. Suter, P.W. Kubik, Production of radionuclides from target elements (Z < 30) by proton-induced reactions between 200 and 400 MeV, Nucl. Instr. Meth. Phys. Res. B (1996) in press.

[7] R. Michel, R. Bodemann, H. Busemann, R. Daunke, M. Gloris, B. Klug, A. Krins, H.-J. Lange, I. Leya, M. Lüpke, S. Neumann, H. Reinhardt , M. Schnatz-Büttgen, U. Herpers, Th. Schiekel, F. Sudbrock, B. Holmqvist, H. Condé, P. Malmborg, M. Suter, B. Dittrich-Hannen, P.-W. Kubik, H.-A. Synal, Cross Sections for the Production of Residual Nuclides by Low- and Medium-Energy Protons from the Target Elements C, N, O, Mg, Al, Si, Ca, Ti, Mn, Fe, Co, Ni, Cu, Nb, Sr, Y, Zr, Nb, Ba and Au, to be submitted to Nucl. Instr. Methods in Phys. Res. B (1996).

[8] C.D. Bowman and 21 coauthors (1992) Nucl. Instr. Meth. Phys. Res. A320 (1992) 336 - 367.

[9] F. Carminati, R. Klapisch, J.P. Revol, Ch. Roche, J.A. Rubio, C. Rubbia, CERN/AT/93-47(ET) (1993).

[10] M. Blann, H. Gruppelaar, P. Nagel, J. Rodens (1994) International Comparison for Intermediate Energy Nuclear Data, NEA/OECD, Paris.

[11] D. Filges, P. Nagel, R.D. Neef (1995) International Intercomparison for Intermediate Energy Nuclear Data - The Thick Target Bench Mark, NSC/DOC (95) 2, NEA/OECD, Paris

[12] Intermediate Energy Nuclear Data: Models and Codes, Proceedings of a Specialists' meeting, Issy-les-Moulineaux (France), 30 May - 1 June 1994, OECD, Paris.

[13] R. Michel, P. Nagel (1995) Specifications of an International Codes and Model Intercomparison for Intermediate Energy Activation Yields, NEA/NSC/DOC (95) 8.

[14] Th. Schiekel, R. Rösel, U. Herpers, I. Leya, M. Gloris, R. Michel, B. Dittrich-Hannen, P.W. Kubik, H.-A. Synal, M. Suter, Cross sections for the p-induced production of longlived radionuclides for the interpretation of cosmogenic nuclides, Nuclear Data for Science and Technology, J.K. Dickens (ed.), pp. 344 - 346 (1994) American Nuclear Society, Inc., La Grange Park, Illinois.

[15] Th.Schiekel, F. Sudbrock, U. Herpers, M. Gloris, I. Leya, R. Michel, H.-A. Synal, M. Suter, On the production of ^{36}Cl by high energy protons in thin and thick targets, Proceedings of the "4th European Conference on Accelerators in Applied Research and Technology", August 29 - Septeber 2, 1995, Zürich, Switzerland, Nucl. Instr. Meth. (1995) in press.

[16] Th.Schiekel, Thesis, Universität zu Köln (1995).

[17] H.H.Anderson and J.F.Ziegler, Hydrogen stopping powers and ranges in all elements, Pergamon Press (1977).

[18] J.Tobailem and C.H. de Lassus St. Genies, CEA-N-1466 (5) (1981).

[19] G.F. Steyn, S.J. Mills, F.M. Nortier, B.R.S. Simpson, B.R. Meyer, Appl. Radiat. Isot. 41 (1990) 315.

[20] U. Neupert, thesis, Universität Hannover (1996).

[21] R.C. Finkel, M. Suter, AMS in the Earth Sciences: Techniques and Applications, Adv. Anal. Geochem. 1 (1993), 1 - 114; H.A.Synal et al., Nucl.Instr. Meth. B52 (1990) 438; H.J.Hofmann et al., Nucl. Instr. Meth. B29 (1990) 32.

[22] M. Gloris, R. Michel, U. Herpers, F. Sudbrock, B. Holmqvist, H. Condé, P. Malmborg, P.W. Kubik, H.-A. Synal, M. Suter. D. Filges, , Proton-Induced Nuclide Production in Heavy Target Elements at Medium Energies, Proceedings 'Second International Conference on Accelerator-Driven Transmutation Technologies and Applications', Kalmar, Sweden (1996) in press.

[23] M. Gloris, R. Michel, U. Herpers, F. Sudbrock, Production of Residual Nuclides from Irradiation of Thin Pb-Targets with Protons up to 1.6 GeV, Proc. ecaart 4, Nucl. Instr. Meth. Phys. Res. B (1996) in press.

INSTITUT FÜR KERNCHEMIE
UNIVERSITÄT MAINZ

1. Yields of Heavy Ternary Products in the Thermal Neutron Induced Fission of ^{249}Cf

M. Davi, O. Alhassanieh, H. R. Faust, J. O. Denschlag

The fraction of fission reactions, producing three charged particles rather than two, amounts to about 0.2 %. Of the "ternary particles" 90 % are α-particles. However, some heavier fragments are also formed, though rarely [1]. Since the angular distribution of ternary particles indicates that they originate from the neck region of the compound nucleus at scission, their formation ratios and emission characteristics may be used to probe the role of the neck in the fission process and hence to check modern theories, like the theory of multimodal fission [2]. This theory explains the hitherto unexplained large width of the mass distribution curves in fission, by the "Plateau-Rayleigh instability" of a cylindrical neck, known from fluid dynamics.

The high sensitivity and high selectivity of the Lohengrin mass separator of the ILL (Grenoble, France) combined with an ionization chamber with split anode allows to detect ternary fragments of yields down to 10^{-6} % and to identify their mass and nuclear charge. The fissile isotope ^{249}Cf was chosen as target material since the cross section for ternary fission and the fraction of heavy ternary fragments are both expected to be relatively high.

The separation of fission fragments in Lohengrin takes place according to the ratio of their mass to ionic charge (A/q), where q is established in a dynamic equilibrium in this separator for unstopped fission fragments when the fragments penetrate through the target and the covering nickel foil. In the separation Lohengrin selects fragments of identical velocity.

A typical spectrum is shown in Fig. 1. Single events are shown as points clustering in dark spots on a matrix formed by a plot of the specific energy loss of the fragments versus their kinetic energy (both measured in the ionization chamber with split anode). Since the separation in Lohengrin provides frag-

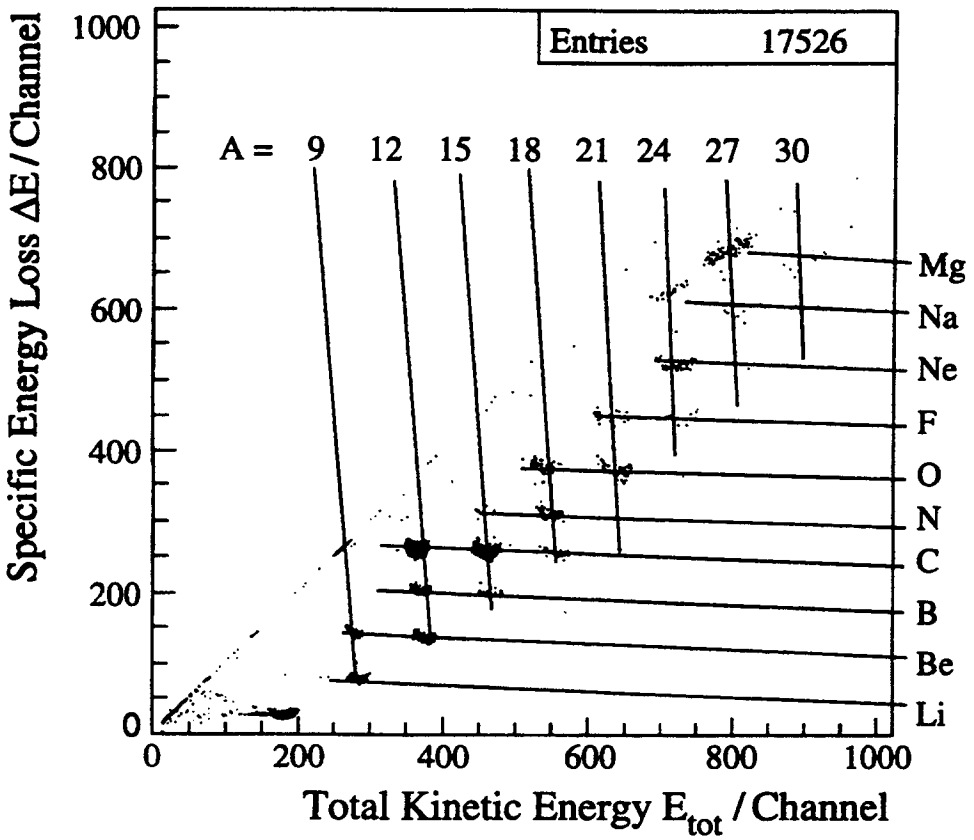

Fig. 1 "Scatter plot" of events registered in the ionization chamber with split anode (at a Lohengrin setting A/q=3 and E/q=3.6 [MeV]). The specific energy loss (ΔE) is plotted versus the total kinetic energy (E_{tot}) of the fragments. Relative intensities are obtained by integrating the events registered in an appropriate area of the matrix.

ments of identical velocity, their total energy (x axis) is a linear function of their mass. The figure shows that the different masses (marked A=9 up to A=30 and representing the ratios A/q = 3, i.e. 9/3 up to 30/10 at kinetic energies corresponding to E/q=3.6 [MeV]) are well separated. The specific energy loss is measured in a first part of the (split) anode, along which the fragments deposit about 60 % of their total kinetic energy. The specific energy loss depends on the nuclear charge of the fragments and allows the identification of their atomic number. The different elements identified are indicated on the right hand side of Fig. 1. Within the total number of spectra measured 37 nuclides ranging up to ^{33}Al could be identified as ternary fission products in $^{249}Cf(n_{th},f)$.

Relative count rates are obtained by summing all events in an appropriate area of the ΔE versus E_{tot} matrix. In order to obtain absolute or relative particle

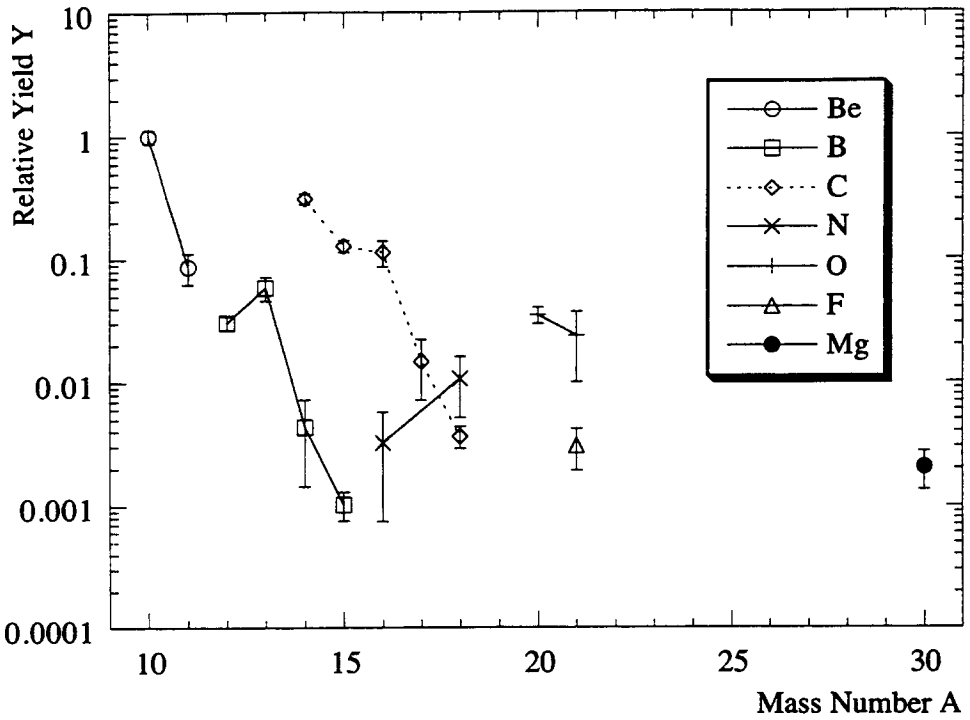

Fig. 2 Yields of ternary particles relative to $^{10}Be=1$ obtained as discussed in the text. The absolute yield of ^{10}Be amounts to $(4 \pm 1)\cdot 10^{-3}$ %

yields every nuclide has to be measured at different kinetic energies and ionic charge states and an integration over the kinetic energy and ionic charge distributions has to be carried out. So far kinetic energy distributions have been measured for 17 nuclides. Approximating the ionic charge distributions by a model of Nikolaev and Dmitriev [3] yields relative to $Y(^{10}Be)=1$ as shown in Fig. 2 were obtained. They may be converted to approximate absolute yields using the yield value of ^{10}Be of $(4 \pm 1)\cdot 10^{-3}$ %, calculated on the basis of the present work and the data of Hentzschel [4]. Further measurements to confirm the predicted ionic charge distribution and to obtain kinetic energy distributions for the other nuclides identified are planned.

[1] W. Baum, S. Neumaier, U. Nast-Linke, A. Göpfert, M. Mutterer, J. P. Theobald, C. Zöller, G. Barreau, T. P. Doan, B. Leroux, A. Sicre, H. Faust, F. Gönnenwein, in C. Wagemans (Ed.): Proceedings of the Seminar on Fission, Pont d'Oye II, October 1991, page 78-87

[2] U. Brosa, S. Grossmann: Z. Phys. A310, 177 (1983)

[3] V.S. Nikolaev, I. S. Dmitriev: Phys. Lett. A28, 277 (1968)

[4] R. Hentzschel: Massen- und Energieverteilung in der Spaltung von ^{249}Cf, Dissertation, Mainz (1992).

FRM-REAKTORSTATION GARCHING
FACHBEREICH PHYSIK
TECHNISCHE UNIVERSITÄT MÜNCHEN

1. Fundamental Properties of the Neutron

Neutron-Electron Scattering Length and Electric Polarizability of the Neutron Derived from Cross Sections of Bismuth and of Lead and its Isotopes.

L. Koester, W. Waschkowski,
L.V. Mitsyna[1], G.S. Samosvat[1],
P. Prokofjevs[2], J. Tambergs[2]

The electric properties of the neutron have been deduced from precise measurements of coherent scattering lengths and of total cross section of Pb, its isotopes with A = 208, 207, and 206, and of Bi. Their energy dependences are due to nuclear properties, nuclear and atomic charges, the electric polarizability of the neutron as well as due to the neutron-electron interaction. We investigated in detail the different evaluations used in the past by German and Russian groups. By means of both data handling methods we found consistent results of $\alpha_n = (0.0 \pm 0.5) \times 10^{-3}$ fm^3 for the electric polarizability and of $b_{ne} = (1.32 \pm 0.03) \times 10^{-3}$ fm^3 for the neutron-electron scattering length. This result agrees with quark-core models of the neutrons.

Published in Phys. Rev. **C 51**, No. 6 (1995).

2. Absorption Cross Section

Absorption Cross Section Measurements with Cold Neutrons on Solid and Powder Samples

K. Knopf, W. Waschkowski

Transmission measurements with cold neutrons of mean energy 0.57 meV on solid and powder samples were performed to deduce the absorption cross sections σ_γ for 43 chemical elements and 27 of their isotopes. The inelastic scattering cross sections σ_{inel} or the Debye-temperature θ_D could be calculated with the data.

---

1 Joint Inst. for Nucl. Research, Frank Lab., 141980 Dubna, Russia
2 Latvian Acad., Nucl. Research Center, L.V-2169 Salaspils, Latvia

Compilation of measured and deduced absorption cross sections:

Meaning of symbols:

σ_{tot}	total cross section at energy E
σ_{inc}	incoherent cross section
σ_{inel}	inelastic cross section
σ_o	free coherent cross section at E = 0
σ_γ	absorption cross section at E = 0.0253 eV
θ_D	Debye-temperature

Z	Sample	σ_o(free) b	σ_γ[a] b	σ_{inc}(free) b	E meV	σ_{tot}(E) b	σ_{inel}(E) b	$\sigma_{\gamma,tot}$(E) b	σ_γ[b] b	Ref.	Θ_D K
11	Na	3.03(2)	0.530(5)	1.52(4)						/6/	158 /3/
	$NaNO_3$	24.3(1)	2.43(3)	1.9(1)	0.48(2)	25.6(3)	6.1(4)				450(30)
	Na_2SO_4	22.07(6)	1.58(2)	3.05(4)	0.48(2)	19.1(4)	4.6(5)				470(50)
12	Mg	3.414(1)	0.063(3)	0.064(20)						/6/	
	solid				0.50(2)	1.46(3)	0.61(6)	0.79(7)	0.111(10)		400 /3/
	solid				0.50(2)	1.46(3)	0.74(7)	0.66(8)	0.093(11)		330 /9/
								mean value:	0.102(7)		
	solid				0.50(2)	1.46(3)	0.95(1)	0.45(4)	0.063(3)		250(10)
	MgF_2	10.67(4)	0.082(3)	0.07(2)	0.68(2)	2.3(1)	1.7(1)				450(20)
	$MgSO_4$	19.42(4)	0.58(2)	0.07(2)	0.50(2)	15.6(2)	11.2(1)				143(6)
13	Al	1.413(12)	0.231(3)	0.023(11)						/6/	
	solid				0.68(2)	1.72(3)	0.18(2)	1.52(4)	0.249(8)		428 /3/
	solid				0.68(2)	1.72(3)	0.21(2)	1.49(4)	0.244(8)		365 /10/
	solid				0.50(2)	1.96(5)	0.22(2)	1.73(6)	0.243(9)		428 /3/
	solid				0.50(2)	1.96(5)	0.25(2)	1.69(6)	0.237(9)		365 /10/
								mean value:	0.243(4)		
14	Si	2.044(2)	0.171(3	0.017(6)						/7/	640 /3/
	poly crystal				0.50(2)	1.43(1)	0.18(2)	1.23(3)	0.173(5)		
					0.55(2)	1.39(1)	0.17(2)	1.20(2)	0.177(5)		
								mean value:	0.175(4)		
	SiO_2										470 /3/
	α-quartz	9.57(1)	0.171(3)	0.017(6)	0.50(2)	3.05(2)	1.81(8)				510(10)
	nat.opal	9.57(1)			0.57(2)	4.88(6)	3.72(6)				225(10)
	single crystal	9.57(1)			0.50(2)	6.15(10)	4.90(15)				170(10)
15	P	3.13(1)	0.172(2)	0.02(2)						/11/	
	red cryst. powder				0.57(2)	3.0(2)	1.8(2)				55(10)
16	S	0.964(6)	0.52(1)	0.006(6)						/7/	
	cryst. powder				0.51(2)	4.76(2)	1.08(3)				19(2)
	cryst. powder				0.51(2)	4.30(7)	0.63(10)				48(11)

a) $\sigma_\gamma = \sigma(0.0253\ eV)$ from /2/,
b) σ_γ deduced from this measurements.
c) unpublished.

Continued

Z	Sample	σ_0(free) b	σ_γ [a] b	σ_{inc}(free) b	E meV	σ_{tot}(E) b	σ_{inel}(E) b	$\sigma_{\gamma,tot}$(E) b	σ_γ [b] b	Ref	Θ_D K
20	Ca	2.76(2)	0.43(2)	0.025(3)						/12/2/	230 /3/
	CaF_2										510 /3/
	single crystal	10.02(5)	0.45(2)	0.031(34)	0.50(2)	4.7(1)	1.5(2)	3.2(2)	0.44(3)[c]		510
					0.55(2)	4.56(3	1.4(2)	3.1(2)	0.45(3)[c]		510
								mean value:	0.45(2)		
	cryst. powder				0.60(2)	5.8(4)	2.9(4)				250(50)[c]
					0.50(2)	5.5(1)	2.5(1)				290(20)[c]
									mean value:		270(25)
	$CaCO_3$	18.78(3)	0.43(2)	0.032(6)	0.52(2)	7.8(1)	4.7(2)				420(15)[c]
	$CaSO_4$	18.78(3)	0.95(2)	0.031(7)	0.51(2)	12.0(2)	5.3(3)				340(20)[c]
22	Ti	3.822(9)	6.09(13)	2.45(1)						/13/	420 /3/
	solid				0.560(7)	46.1(2)	0.31(3)	43.3(2)	6.44(5)		420
	TiO_2	11.34(2)	6.09(13)	2.45(1)	0.55(2)	46.1(4)	1.0(2)	42.6(4)	6.28(12)[c]		760 /3/
					0.50(2)	47.3(5)	1.1(2)	43.7(5)	6.14(12)[c]		760 /3/
	$TiSi_2$	7.91(3)	6.61(9)	2.47(1)	0.55(2)	55.6(6)	9.5(6)	43.6(8)	6.25(16)[c]		18(2)
								mean value:	6.28(6)		
23	V	4.813(5)	5.08(4)	4.58(1)						/13/	360 /3/
	solid				0.560(7)	39.28(9)	0.43(4)	34.27(13)	5.10(3)		360
	V_2O_5	28.43(4)	10.16(8)	9.16(2)	0.57(2)	78(2)	0	69(2)	5.17(16)[c]		
								mean value:	5.14(7)		
24	Cr	3.38(1)	3.07(8)	1.78(2)						/14/	639 /3/
	met. powder				0.50(2)	23.6(3)	0.16(2)	21.7(3)	3.05(6)		639
	Cr_2O_3	18.05(3)	6.14(16	3.64(4)	0.50(2)	51.2(5)	4.3(5)				340(40)
25	Mn	2.03(3)	13.3(2)	0.32(3)						/13/	450 /3/
	met. powder				0.57(2)	84(2)	0.14(2)	83.5(2.0)	12.3(4)		450
27	Co	5.74(5)	37.18(6)	4.99(5)						/15/12/	445 /3/
	CoF_2-solid	13.00(6)	37.20(6)	5.00(5)	0.53(2)	267(3)					
	cryst. Powder				0.53(2)	263(3)					
					mean value:	265(2)	3(1)	260(2)			230(180)[c]
28	Ni	17.8(3)	4.49(16)	5.00(5)						/2/	450 /3/
	solid				0.560(7)	35.9(1)	1.1(1)	29.8(4)	4.43(8)[c]		450
29	Cu	7.86(8)	3.78(2)	0.58(4)						/12/16/	343 /3/
	solid				0.553(7)	26.74(12)	0.60(5)	25.56(14)	3.78(3)[c]		343

a) $\sigma_\gamma = \sigma$(0.0253 eV) from /2/,
b) σ_γ deduced from this measurements,
c) unpublished.

Continued

Z	Sample	σ_0(free) b	σ_γ[a] b	σ_{inc}(free) b	E meV	σ_{tot}(E) b	σ_{inel}(E) b	$\sigma_{\gamma,tot}$(E) b	σ_γ[b] b	Ref.	Θ_D K
30	Zn	4.00(1)	1.11(2)	0.05(2)						/17/	310 /3/
	met. powder				0.56(2)	7.98(8)	0.32(3)	7.561(9	1.13(2)		310
	ZnO	7.76(2)	1.11(2)	0.05(2)	0.56(2)	8.86(13)	1.4(2)				360(40)
	^{64}ZnO	7.08(4)	0.76(2)	0	0.56(2)	8.9(4)	1.4(2)	7.2(4)	1.07(6)		
	^{66}ZnO	8.11(5)	0.85(20)	0	0.56(2)	5.6(5)	1.4(2)	4.2(5)	0.62(7)		
31	Ga	6.94(2)	2.9(1)	0.46(3)						/18/	
	solid				0.56(1)	19.8(2)	0.51(5)	18.8(2)	2.80(4)		320 /3/
	solid				0.56(1)	19.8(2)	0.68(7)	18.7(2)	2.78(4)		228 /19/
								mean value:	2.79(3)		
	GaP	10.07(3)	2.95(4)	0.48(2)	0.56(1)	21.5(2)	1.1(2)				290(50)
	Ga_2O_3	25.16(7)	5.56(8)	0.92(6)	0.56(1)	44.5(3)	6.1(4)				230(20)
	$^{69}Ga_2O_3$	27.4(3)	3.36(14)	1.0(3)	0.56(1)	37.2(8)	6.1(4)	30.6(9)	2.28(8)		
	$^{71}Ga_2O_3$	21.6(5)	9.4(4)	0.3(5)	0.56(1)	57(2)	6.1(4)	51(2)	3.79(16)		
								$\sum \sigma_{i,ch_i}$ = 2.88(8)			
32	Ge	8.53(2)	2.3(2)	0.35(3)						/20/	
	solid				0.57(2)	15.7(2)	0.52(5)	14.9(2)	2.24(5)		370 /3/
	solid				0.57(2)	15.7(2)	0.65(6)	14.7(2)	2.21(5)		290 /21/
								mean value:	2.23(4)		
	GeO_2										
	amorph.	16.05(2)	2.23(5)	0.35(3)	0.57(2)	23.0(6)	7.8(6)				99(12)
	tetragonal			0.35(3)	0.57(1)	17.1(6)	2.0(6)				480(120)
	hexagonal			0.35(3)	0.57(2)	16.0(4)	0.9(4)				870(230)
33	As	5.36(4)	4.5(1)	0.06(4)						/22/	
	GaAs	12.30(5)	7.3(1)	0.52(3)	0.56(2)	47.9(2)	1.1(1)	46.3(2)	4.11(13)[c]		247 /23/
	As_2O_3	22.00(7)	8.2(3)	0.12(8)	0.51(2)	75.3(6)	17.5(7)				63(3)
34	Se	8.12(10)	11.7(2)	0.34(10)						/22/	90 /3/
	met. powder				0.48(2)	86.0(7)	1.51(11	84.2(7)	11.6(2)		90
37	Rb	6.24(4)	0.38(4)	0.07(5)							
	RbBr	12.1(1)	7.3(2)	0.4(1)	0.51(2)	51(1)	0	51(1)	6.8(2) for Br		
	RbJ	10.03(8)	6.6(2)	0.38(8)	0.51(2)	48(1)	0	48(1)	6.4(2). for J		
	Rb_2SO_4	28.48(7)	1.28(8)	0.16(10)	0.51(2)	16(1)	7(1)				280(50)
38	Sr	6.08(2)	1.28(6)	0.026(4)						/8/	147 /3/
	SrF_2										
	single cryst.	13.34(5)	1.30(6)	0.03(2)	0.51(2)	9.1(2)	0	9.1(2)	1.29(3)[c]		
	cryst. powder				0.51(2)	11.0(5)	1.9(5)				420(100)
	$SrCO_3$	22.10(4)	1.28(6)	0.033(6)	0.51(2)	14(1)	5(1)				410(80)

a) $\sigma_\gamma = \sigma(0.0253\ eV)$ from /2/,

b) σ_γ deduced from this measurements,

c) unpublished.

Continued

Z	Sample	σ_0(free) b	σ_γ [a] b	σ_{inc}(free) b	E meV	$\sigma_{tot}(E)$ b	$\sigma_{inel}(E)$ b	$\sigma_{\gamma,tot}(E)$ b	σ_γ [b] b	Ref.	Θ_D K
39	Y	7.54(9)	1.28(2)	0.16(8)						/8/	
	Y_2O_3	26.36(18)	2.56(4)	0.32(16)	0.68(2)	28.5(2)	12.6(3)				84(6)
40	Zr	6.42(5)	0.185(3)	0.13(8)						/8/	
	solid				0.51(2)	1.97(4)	0.39(3)	1.45(9)	0.206(13)		310 /3/
					0.51(2)	1.97(4)	0.55(1)	1.29(9)	0.183(13)		205 /10/
								mean value:	0.195(9)		
	ZrO_2	13.94(6)	0.185(3)	0.13(8)	0.51(2)	2.7(2)	1.2(2)				670(70)
41	Nb	6.23(5)	1.15(5)	0.006(1)						/24/2/	230 /3/
	solid				0.58(2)	7.7(1)	0.45(4)	7.2(1)	1.09(2)[c]		230
42	Mo	5.54(2)	2.55(5)	0.01(3)						/25/	
	poly crystal				0.54(2)	17.4(1)	0.21(1)	17.18(12)	2.51(5)		450 /3/
							0.24(2)	17.15(12)	2.51(5)		407 /26/
	met. powder				0.55(2)	17.06(3)	0.21(1)	16.84(5)	2.49(4)		450 /3/
							0.23(2)	16.82(5)	2.49(4)		407 /26/
								mean value:	2.50(2)		
	MoO_3	16.82(4)	2.50(3)	0.01(3)	0.57(2)	21.8(3)	5.2(3)				230(20)
					0.55(2)	20.4(2)	3.5(2)				370(20)
	$^{92}MoO_3$	17.2(1)	0.019	0	0.56(2)	6.4(2)	5.0(2)	1.4(3)	0.20(4) [c]		
	$^{94}MoO_3$	17.01(8)	0.015	0	0.56(2)	8.7(79	5.0(2)	3.7(7)	0.55(10)[c]		
	$^{95}MoO_3$	17.19(7)	14.0(5)	0	0.56(2)	92.9(6)	5.0(2)	87.9(6)	13.1(3) [c]		
	$^{96}MoO_3$	16.05(7)	0.5(2)	0	0.56(2)	8.8(1.0)	5.0(2)	3.8(1.0)	0.56(15)[c]		
	$^{97}MoO_3$	17.8(1)	2.1(5)	0	0.56(2)	20.3(7)	5.0(2)	15.3(7)	2.3(1) [c]		
	$^{98}MoO_3$	16.64(8)	0.25(13	0	0.56(2)	5.9(79	5.0(2)	0.9(7)	0.13(11)[c]		
	$^{100}MoO_3$	16.90(8)	0.199(3)	0	0.56(2)	6.9(2)	5.0(2)	1.9(3)	0.28(4) [c]		
					$\sum \sigma_i \times h_i$=21.8(3)		5.0(3)	16.3(4)	2.50(7)		240(20)
44	Ru	6.07(2)	2.56(13)	0						/27/	600 /3/
	met. powder				0.48(2)	17.9(3)	0.17(2)	17.7(3)	2.44(6)		600
	RuO	9.83(5)	2.56(13)	0	0.55(2)	17.0(3)	0.5(3)	16.5(6)	2.43(9)		340(270)
								mean value:	2.44(5)		

a) $\sigma_\gamma = \sigma$(0.0253 eV) from /2/.

b) σ_γ deduced from this measurements.

c) unpublished.

Continued

Z	Sample	σ_0(free) b	σ_γ [a] b	σ_{inc}(free) b	E meV	σ_{tot}(E) b	σ_{inel}(E) b	$\sigma_{\gamma,tot}$(E) b	σ_γ [b] b	Ref.	Θ_D K
50	Sn	4.81(2)	0.626(9)	0.02(2)						/28/	
	solid				0.558(6)	4.16(2)	0.31(3)	3.83(4)	0.569(8)		199 /3/
							0.34(3)	3.80(4)	0.564(8)		175 /29/
								mean value:	0.567(6)		
	SnO_2										
	amorph.	12.33(2)		0.02(2)	0.553(9)	7.5(3)	3.7(2)				217(15)
	tetragonal				0.553(9)	6.2(2)	2.4(2)				360(30)
	β-modification				0.553(9)	7.8(6)	4.0(6)				195(45)
	^{116}SnO	12.13(4)	0.14(3)		0.553(9)	8.0(7)	4.7(3)	3.3(8)	0.49(10) [c]		
	^{117}SnO	12.89(5)	2.3(5)		0.553(99	9.8(3)	4.7(3)	5.1(4)	0.75(6) [c]		
	^{118}SnO	12.32(4)	0.22(5)		0.553(9)	6.2(2)	4.7(3)	1.5(4)	0.22(6) [c]		
	^{119}SnO	12.43(8)	2.2(5)		0.553(9)	19.4(7)	4.7(3)	14.7(8)	2.17(12) [c]		
	^{120}SnO	13.02(4)	0.14(3)		0.553(9)	8.3(2)	4.7(3)	3.6(4)	0.53(6) [c]		
	^{122}SnO	11.89(9)	0.18(2)		0.553(9)	5.9(2)	4.7(3)	1.2(4)	0.18(5) [c]		
	^{124}SnO	12.19(4)	0.13(1)		0.553(9)	7.3(3)	4.7(3)	2.6(4)	0.38(6) [c]		
					$\sum \sigma_i x h_i$ = 8.5(3)		4.7(3)	3.87(3)	0.57(7)		156(15)
51	Sb	3.87(6)	5.1(1)	0.03(5)						/30/	
	solid				0.56(2)	33.0(2)	0.24(2)	32.7(2)	4.86(9)		207 /3/
							0.25(2)	32.7(2)	4.86(9)		182 /19/
								mean value:	4.86(6)		
	Sb_2O_4	22.82(12)	9.72(12)	0.06(10)	0.55(2)	74.6(9)	8.7(9)				170(25)
	$^{121}Sb_2O_4$	23.10(12)	11.8(4)	0	0.55(2)	86.3(9)	8.7(9)	77.6(1.0)	5.75(12)		
	$^{122}Sb_2O_3$	22.20(10)	8.4(2)	0	0.55(2)	59(3)	8.7(5)	50(3)	3.69(2)		
								$\sum \sigma_i x h_i$ = 4.9(2)			
52	Te	4.25(4)	4.7(1)	0.08(4)						/30/	
	solid				0.568(9)	27.4(2)	0.31(3)	27.0(5)	3.91(7)		153 /3/
							0.35(3)	27.0(5)	3.91(7)		132 /31/
								mean value:	3.91(5)		
	TeO_2										
	tetragonal	11.77(5)	3.91(8)	0.09(1)	0.57(2)	33.5(5)	7.4(6)				86(10)
53	J	3.76(7)	6.2(2)	0.31(6)						/30/	
	C_2J_4	24.4(3)	24.9(8)	0.62(12)	0.57(2)	175(1)	8.7(1)				145(25)

a) $\sigma_\gamma = \sigma$(0.0253 eV) from /2/.

b) σ_γ deduced from this measurements.

c) unpublished.

Continued

Z	Sample	σ_0(free) b	σ_γ [a] b	σ_{inc}(free) b	E meV	σ_{tot}(E) b	σ_{inel}(E) b	$\sigma_{\gamma,tot}$(E) b	σ_γ [b] b	Ref.	Θ_D K
56	Ba	3.27(5)	1.2(1)	0.09(7)						/32/	110 /3/
	BaF_2										
	single cryst.	10.53(6)	1.2(1)	0.10(7)	0.57(2)	9.24(7)	1.0(1)				610(40)
	$BaCO_3$	19.29(6)	1.2(1)	0.10(7)	0.57(2)	13.4(4)	5.3(4)				350(30)
74	W	4.54(12)	18.4(3)	1.60(12)						/33/	
	single cryst.				0.568(9)	115.4(5)	0.10(1)	113.7(6)	17.0(2)		400 /3/
							0.17(2)	113.6(6)	17.0(2)		220 /34/
	WO_3	15.82(4)	18.4(3)	1.60(12)	0.532(9)	119.8(5)	0	118.1(5)	17.1(2)		
								mean value:	17.0(1)		
	$^{182}WO_3$	17.44(6)	20.7(5)		0.57(2)	131(2)	0	131(2)	19.6(3)		
	$^{183}WO_3$	16.68(6)	10.1(3)	0.5(2)	0.57(2)	70(2)	0	70(2)	10.5(2)		
	$^{184}WO_3$	18.46(22)	1.7(1)		0.57(2)	11.5(8)	0	11.5(8)	1.7(1)		
	$^{186}WO_3$	11.94(6)	37.9(6)		0.57(2)	257(5)	0	275(5)	38.5(8)		
								$\sum \sigma_{partial}$=	18.2(4)		
81	Tl	9.63(2)	3.46(3)	0.048(5)						/27/	87 /3/
	Tl_2O_3	30.54(6)	6.92(6)	0.096(10)	0.56(2)	55.2(8)	8.6(9)				124(10)
82	Pb	11.02(6)	0.171(2)	0.007(56)						/35/	110 /3/
	solid				0.556(5)	1.717(15)	0.614(54)	1.096(78)	0.162(12)		110
							0.56(7)	1.16(7)	0.172(9)		126(23)[c]
	^{208}Pb solid-I	11.23(10)	0.00049(3)		0.556(5)	0.755(14)	0.75(3))				81(3)[c]
	^{208}Pb solid-II	11.23(10)	0.00049(3)		0.556(5)	0.875(25)	0.88(3)				63(3)[c]
	^{206}PbO	14.37(8)	0.0306(8)		0.59(2)	9(1)	9(1)				26(4)[c]
	^{207}PbO	14.47(7)	0.712(10)		0.59(2)	14(2)	9(2)				24(8)[c]
	^{208}PbO	15.58(14)	0.00049(3)		0.59(2)	6.4(8)	6.4(9)				43(9)[c]
									mean value PbO:		31(6)
56	Th	13.24(5)	7.37(6)							/36/	
	solid				0.55(2)	50.2(6)	0.49(5)	49.7(6)	7.33(15)		170 /3/
							0.41(4)	49.8(6)	7.34(15)		200 /37/
								mean value:	7.34(11)		

a) $\sigma_\gamma = \sigma$(0.0253 eV) from /2/.

b) σ_γ deduced from this measurements.

c) unpublished.

References

1 K.Binder, Phys. Status Solidi **41**, 767 (1970).
2 S.F.Mughabghab, M.Divadeenam, N.E.Nolte, Cross Section Vol.1,Part A, Acedemic Press Inc. 1981, S.F.Mughabghab, Cross Section Vol.1, Part B, Academic Press Inc. 1984.
3 American Institute of Phys.Handbook, second Edition,McGraw -Hill Book Company, Inc. N.Y. 1963.
4 W.Dilg,W.Mannhart , E.Steichele, Z.Phys. **264**, 427 (1973).
5 W.Dilg,W.Mannhart , Z.Phys. **266**, 157 (1974).
6 L.Koester, K.Knopf, W.Waschkowski, Z.Phys.A **292**, 95 (1979).
7 L.Koester, K.Knopf, W.Waschkowski, Z.Phys.A **289**, 399 (1979).
8 L.Koester, K.Knopf, W.Waschkowski, Z.Phys.A-Atoms a. Nuclei **301**, 215 (1981).
9 Y.S.Touloukian, D.P.DeWitt, Thermophysical Properties of Matter, Vol.1 N.Y. IFI/Plenum 1970.
10 G.L.Squires, Phys.Rev. **103**, 304 (1956).
C.B.Walker, Phys.Rev. **103**, 547 (1956).
11 L.Koester, K.Knopf, W.Waschkowski, Z.Phys.A **277**, 77 (1976).
12 L.Koester, H.Rauch, E.Seymann, Atomic Data a. Nuclear Data Tables **49**, 65 (1991).
13 L.Koester, K.Knopf, W.Waschkowski, Z.Phys.A **345**, 176 (1993).
14 L.Koester, K.Knopf, W.Waschkowski, Z.Phys.A **287**, 61 (1978).
15 L.Koester, K.Knopf, W.Waschkowski, Z.Phys.A **271**, 201 (1974).
16 J.P. Niklaus, R.Simson, W.Triftshäuser, W.Schmatz, Z.Phys. **190**, 295 (1966)
17 L.Koester, K.Knopf, W.Waschkowski, Z.Phys.A-Atoms a. Nuclei **320**, 661 (1985).
18 L.Koester, K.Knopf, W.Waschkowski, Z.Phys.A-Atoms a. Nuclei **318**, 347 (1984).
19 J.F.Tibballs, S.M.Feteris, S.M.Barnea. Z.Aust.J.Phys. **34**, 689 (1981).
20 L.Koester, K.Knopf, W.Waschkowski, Z.Phys.A-Atoms a. Nuclei **327**, 129 (1987)
21 B.W.Battermann, D.R.Chipman, Phys.Rev.**127**, 690 (1962).
22 L.Koester, K.Knopf, W.Waschkowski, Z.Phys.A-Atoms a. Nuclei **296**, 43 (1980).
23 G.Arnold, N.Nereson, Phys.Rev. **131**, 2098 (1963).
24 L.Koester, K.Knopf, Z.Naturforsch. **26a**, 399 (1971).
25 L.Koester, K.Knopf, W.Waschkowski, Z.Phys.A-Atom a. Nuclei **326**, 227 (1987).
26 T.Paakari, Acta Cryst. **A30**, 83 (1973).
27 K.Knopf, W.Waschkowski, Z.Phys. A **352**, 449 (1995)
28 K.Knopf, W.Waschkowski, to be published.
29 Y.S.Touloukia, F.H.Buco, Thermophysical Properties of Matter, Vol.4, /F/ Plenum 1970.
30 L.Koester, K.Knopf, W.Waschkowski, Z.Phys.A-Atomic Nuclei **323**, 359 (1986).
31 Gmelin, Handbook of Inorganic Chemistry: Te, Suppl.A2, Berlin, Heidelberg, N.Y., Springer 1983.
32 L.Koester, K.Knopf, W.Waschkowski, Z.Phys.A-Atoms a. Nuclei **322**, 105 (1985).
33 K.Knopf, W.Waschkowski, Z.Naturforsch. **42a**, 909 (1987).
34 Gmelin, Handbuch der anorganischen Chemie, W-Erg.Bd. (B2), Weinheim 1979.
35 L.Koester, K.Knopf, Z.Phys.A-Hadrons a. Nuclei **338**, 233 (1991).
35 W.Waschkowski, K.Knopf, Z.Naturforsch. **44**, 174 (1989).
37 Gmelin, Handbuch der anorganischen Chemie, Th-Erg.Bd.C1, Berlin, Heidelberg, Springer 1978.
38 D'ans Lax, Taschenbuch für Chemiker u. Physiker, Bd.I, Berlin, Heidelberg, Springer 1967.
39 L.Koester, K.Knopf, Z.Phys.A-Atomic Nuclei **323**, 367 (1986).
40 C.O.Fischer, Berichte d. Bunsengesellschaft f. phys. Chemie, **Bd.75**, 361 (1971).
41 J.J.Rush, P.S.Leung, T.LTaylor, J.of Chem.Physics,Vol.45 Nr.4, 1312 (1966).
42 K.Heinloth, Z.Phys. **163**, 218 (1961).

INSTITUT FÜR KERNENERGETIK UND ENERGIESYSTEME (IKE) UNIVERSITÄT STUTTGART

Scattering Laws for Moderators, Reflectors and Filters for Application in Design Calculations of Cold and Superthermal Neutron Sources

W. Bernnat, J. Keinert, M. Mattes, S. Käfer, M. Predel

The optimization of cold neutron sources (e.g. liquid or supercritical H_2,D_2) and superthermal sources (e.g. liquid ^{4}He) is an important task for the efficient generation of cold neutrons in research reactors or spallation sources. For realistic design calculations adequate scattering laws are needed for cold moderators (e.g. H_2 at 20 K, D_2 at 24 K, ^{4}He at 1 K), structure materials (e.g. Al, Mg at about 20 K), filters (e.g. Be at 2–4 K, Pb or Bi at 77 K or room temperature) and reflectors. For the domain of cold neutrons the coherence effects must be considered for these materials, the incoherent approximation is not adequate to the problem. For liquid hydrogen and deuterium we have derived scattering–law data which consider both the intramolecular and intermolecular interference. For supercritical H_2 and D_2, the scattering law can be derived from the Young–Koppel model. For liquid helium (as a source of ultracold neutrons), we connect the atomic neutron scattering with the interatomic interference scattering by a static structure factor. For D bound in D_2O, the intramolecular interference as well as the intermolecular (coherent) neutron scattering is considered. The data for the solid neutron filter materials Be and Bi must include incoherent inelastic and coherent elastic scattering, which is pronounced by the lattice structure. For bismuth, the incoherent part is generated from a frequency distribution, for the coherent part the rhomboedric crystal structure of the lattice is taken into account. For Pb and Al the fcc structure is taken into account. The scattering laws $S(\alpha,\beta)$ for all the mentioned materials are available in ENDF–6 format. As far as possible, the data were validated by comparison of calculated and measured differential and integral cross–sections and neutron flux spectra. As an application, coupled neutron and gamma transport calculations with S_n and Monte Carlo codes for the determination of flux spectra and heat production have been carried out for the planned FRM–II research reactor (Munich). Processed data libraries are available in formats for multigroup transport calculations and formats for the Monte Carlo Transport code MCNP.

PHYSIKALISCH-TECHNISCHE BUNDESANSTALT BRAUNSCHWEIG

1. Neutron Scattering on Natural Chromium at Energies between 8 and 15 MeV

D. Schmidt, W. Mannhart

After iron and lead, chromium has been used to continue the neutron scattering cross section measurements on fusion-relevant materials. There is lack of data in the energy range between 8 and 15 MeV, which may be also due to difficulties in obtaining samples of sufficient purity and density.

Measurements were carried out with a sample of natural chromium at 10 incident energies between 7.95 MeV and 14.76 MeV. The measurement arrangement, data reduction and correction procedures were the same as described for the iron measurement [1].

Data on elastic scattering and inelastic scattering to the first level (E_{ex} = 1.434 MeV) in ^{52}Cr (content 83.79%) had been obtained first. The influence of neighbouring levels of other isotopes (for instance ^{53}Cr) on the inelastic cross sections obtained was estimated at less than 10%. A comparison of the angle-integrated elastic cross sections of this work with data from the literature and evaluations is shown in Fig. 1. Agreement with the EFF-2 evaluation [2] is good, differences to the ENDF/B-VI evaluation are in the order of 5% to 10%. Differences in the differential data may be clearly larger, for instance the inelastic scattering is assumed to be isotropic in the ENDF evaluation.

Below the incident energy of 10 MeV, data were measured at ANL, too, but have not been published until now [3].

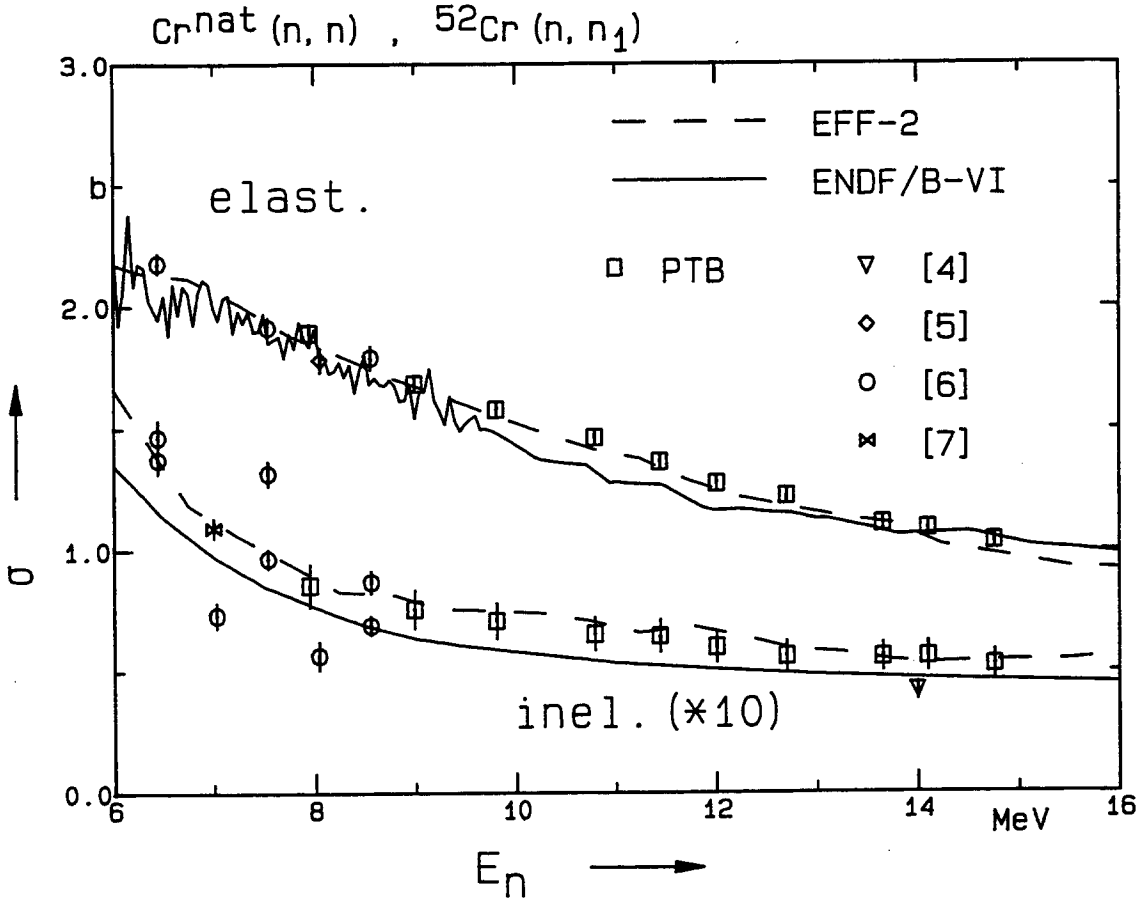

Fig. 1 Angle-integrated elastic cross sections from natural chromium and inelastic cross sections to the first excited state in the ^{52}Cr isotope (note the scale expansion factor of 10); data from the literature [4-7] are included, the EFF-2 and ENDF/B-VI evaluations presented here have been made for the main isotope ^{52}Cr.

2. Activation Cross Section Measurements for Chromium and Vanadium

W. Mannhart, D. Schmidt, D.L. Smith*

The cross sections for $^{51}V(n,p)^{51}Ti$, $^{51}V(n,\alpha)^{48}Sc$, $^{52}Cr(n,p)^{52}V$ and $^{52}Cr(n,2n)^{51}Cr$ were measured at 15 neutron energies between 7.9 and 14.5 MeV. With a deuterium gas target, neutrons were produced via the $D(d,n)^3He$ reaction. The neutron energies were determined with time-of-flight techniques. Metallic samples,

*Argonne National Laboratory, USA

10 mm in diameter and 1 mm thick, were attached to the front of a low-mass fission chamber with a ^{238}U fission deposit acting as neutron fluence monitor. The samples were irradiated at zero degrees with a distance of 6 cm between gas target and samples. The chromium samples required special handling and were fabricated from a chromium sheet by laser cutting. The radioactivity was measured with a calibrated HPGe detector of 300 cm^3. The detailed data analysis is in progress.

References

[1] D. Schmidt et al., Report PTB-N-20, PTB Braunschweig/FRG (1994)

[2] V. Pronyaev et al., Physics Data 13-8, Karlsruhe/FRG (1995)

[3] A.B. Smith, private communication

[4] H.P. Stelson et al., Nucl. Phys. 68 (1965) 97 and EXFOR 11527

[5] B. Holmqvist et al., Nucl. Phys. A 188 (1972) 24 and EXFOR 20019

[6] W.E. Kinney et al., Report ORNL-4806, ORNL Oak Ridge/USA (1974) and EXFOR 10413

[7] I.A. Korzh et al., Ukrain. Fiz. Zhurnal 22 (1977) 87 and EXFOR 40619

APPENDIX

Addresses of Contributing Laboratories

Institut für Kernphysik III
Director: Prof. Dr. G. Schatz
Senior reporter: Dr. F. Käppeler
Forschungszentrum Karlsruhe
Postfach 36 40
76021 Karlsruhe

Institut für Nuklearchemie
Director: Prof. Dr. H.H. Coenen
Senior reporter: Dr. S.M. Qaim
Forschungszentrum Jülich
Postfach 1913
52425 Jülich

Institut für Kern- und Teilchenphysik
Director: Prof. Dr. K.R. Schubert
Senior reporter: Prof. Dr. K. Seidel
Technische Universität Dresden
Mommsenstr. 13
01062 Dresden

Zentrum für Strahlenschutz und Radioökologie
Head and senior reporter: Prof. Dr. R. Michel
Universität Hannover
Am Kleinen Felde 30
30167 Hannover

Abteilung Nuklearchemie
Head: Prof. Dr. H.H. Coenen
Senior reporter: Dr. U. Herpers
Universität zu Köln
Otto-Fischer-Straße 12 - 14
50674 Köln

Institut für Kernchemie
Head and senior reporter: Prof. Dr. J.O. Denschlag
Universität Mainz
Fritz-Strassmann-Weg 2
55128 Mainz

FRM-Reaktorstation Garching
Fachbereich Physik
Senior reporter: Dr. W. Waschkowski
Technische Universität München
85747 Garching/München

Institut für Kernenergetik und Energiesysteme
Director: Prof. Dr. A Schatz
Senior reporter: Dr. W. Bernnat
Universität Stuttgart
Pfaffenwaldring 31
70569 Stuttgart

Physikalisch-Technische Bundesanstalt
Abteilung 7, Neutronenphysik
Director: Prof. Dr. R. Jahr
Senior reporter: Dr. W. Mannhart
Bundesallee 100
38116 Braunschweig